Matrix Metalloproteinase 9 (MMP-9) and Biodegradable Polymers in the Engineering of a Vascular Construct

A Thesis
Presented to
The Academic Faculty

By

Hak-Joon Sung

In Partial Fulfillment
of the Requirements for the Degree
Doctor of Philosophy in the
Department of Biomedical Engineering

Georgia Institute of Technology
June 2004

Matrix Metalloproteinase 9 (MMP-9) and Biodegradable Polymers in the Engineering of a Vascular Construct

Approved by

Dr. Larry V. McIntire, Advisor

Dr. Zorina S. Galis

Dr. Raymond P. Vito

Dr. J. Carson Meredith

Dr. Samuel C. Dudley, Jr.

Date Approved April 16, 2004

ACKNOWLEDGEMENT

This dissertation would not have been possible without the help of many people. I am greatly appreciative of my advisors and teachers Dr. Zorina S. Galis and Dr. Larry V. McIntire, for their patient help and invaluable guidance throughout the course of my graduate studies. I have learned a great deal from their teaching, knowledge, and criticism. I am greatly indebted to them for their continuous encouragement and helpful advice. Because of their instruction and coaching, I was able to finish my thesis.

I would like to thank Dr. J. Carson Meredith as a project co-investigator and committee member, for giving his valuable time and insightful comments. He showed the real engineering aspect to me.

I would also thank Dr. Raymond P. Vito and Dr. Samuel C. Dudley, Jr., as thesis committee members for making my Ph.D. graduate studies priceless and respected.

I extend my special appreciation to Dr. Suzanne G. Eskin for providing helpful advice and instruction.

I hope that my subsequent career makes my committee members proud.

I would also like to express my appreciation to NIH for the funding provided.

My life at Georgia Tech and Emory University, was enriched by many people around me. I owe all the Galis lab members for their intellectual support and advice. Thanks especially to my colleagues, Chad Johnson, Timothy Tolentino, Richard Magid, Harvinder Gill, and Nolan Boyd, with whom I have studied, worked, and played. They made my life enjoyable and meaningful. I am grateful to Andrew Yee for helping me to start work at McIntire lab and for his friendship. Special thanks should also go to Jing Su for his experimental support and help.

I would like to acknowledge my Korean colleagues at Georgia Tech, Yu Shin Kim, Jung Hwan Park, and Gloria Kim, who have accompanied me through the ups and downs of foreign life.

Most importantly, I wish to express my deepest gratitude to my parents. Their support and selfless affection made my studies possible. I am sincerely grateful to my family, my sister and brother-in-law, my elder brother and his wife, my twin and his wife. To all of them, thank you. If it were not for them, this would not have happened. I will do my best to enlighten the future of my lovely nephews, Sang Yun, Bo Yun, Yun Jae, and Yun Suh.

TABLE OF CONTENTS

Acknowledgement iii

List of Tables vii

List of Figures viii

List of Abbreviations x

Summary xii

Chapter 1 Introduction 1

1.1 Overview 1

1.2 Tissue Engineered Vascular Equivalents 3

1.3 Biodegradable Polymers in Vascular Constructs 6

1.4 MMPs in Vascular Remodeling 8

Chapter 2 Objectives 11

2.1 Aim 1 11

2.2 Aim 2 13

2.3 Aim 3 15

Chapter 3 The Effect of Scaffold Degradation Rate on Three-Dimensional Cell Growth and Angiogenesis 17

3.1 Abstract 17

3.2 Introduction 19

3.3 Materials and Methods 20

3.4 Results 24

3.5 Figures and Legends 28

3.6 Discussion 35

Chapter 4 Matrix Metalloproteinase (MMP)-9 Facilitates Cell-Matrix Interactions for Function and Survival of Vascular Constructs 38

4.1 Abstract 38

4.2 Introduction 40

4.3 Materials and Methods 41

4.4 Results 46

4.5 Figures and Legends 50

4.6 Discussion 55

Chapter 5 Combinatorial Screening of Differential Regulation of Cell Interactions on the Surface of Biodegradable Polymer Blends 57

5.1 Abstract 57

5.2 Introduction 58

5.3 Materials and Methods 59

5.4 Results 64

5.5 Figures and Legends 71

5.6 Discussion 83

Chapter 6 Overall Conclusion 86

Chapter 7 Future Studies 89

References 91

Vita 101

LIST OF TABLES

Supplemental Table 1. Comparison of the properties between PLGA and PCL used in this study. 78

LIST OF FIGURES

Figure 1. PLGA can be used to create thin porous scaffolds of uniform thickness. 28

Figure 2. Detection of cell viability using primary cultured mouse aortic smooth muscle cells (MASMC). 29

Figure 3. Cell viability within scaffolds (three dimensional, 3D) decreased with depth and as a function of time. 30

Figure 4. Characterization of PLGA and PCL scaffolds degradation *in vitro* and *in vivo*. 31

Figure 5. Analysis of cell population of biodegradable scaffolds PLGA (right panel) and PCL (left panel) implanted *in vivo* was determined initially (day 0) and at 14 and 28 days (frozen sections). 33

Figure 6. Effect of MMP-9 on collagen production and degradation on TCPS. 50

Figure 7. MMP-9 deficiency does not alter polymer degradation but increases collagen accumulation in PCL scaffolds. 51

Figure 8. Effects of ascorbic acid treatment on collagen production and assembly. 52

Figure 9. *In vivo* host reaction to implanted scaffolds. 53

Figure 10. *In vivo* angiogenesis. 54

Figure 11. Characterization of phase-separated microstructures and surface roughness. 71

Figure 12. SMC adhesion and population distribution. 73

Figure 13. Area dependent SMC populations are linked to proliferation rates. 74

Figure 14. SMC aggregation correlated with surface hardness and crystallinity. 75

Figure 15. Surface composition dependent protein accumulation from culture medium and SMC protein production. 76

Figure 16. Verification of combinatorial libraries SMC adhesion and proliferation using individual uniform films. 77

Supplemental Figure 1. SMC viability decreased at high PLGA compositions. 79

Supplemental Figure 2. Mechanical properties of blended PLGA/PCL were dependent on ΦPCL. 80

Supplemental Figure 3. Crossed-polar optical microscopy reveals changes in crystalline microstructure following SMC culture. 81

Supplemental Figure 4. After 14 days of culture, SMC populations on the combinatorial chip coincided with areas of high protein production. 82

LIST OF ABBREVIATIONS

AFM: Atomic force microscopy

ANOVA: Analysis of variation

CABG: Coronary artery bypass graft surgery

CAD: Coronary artery disease

DSC: Differential scanning calorimeter

EC: Endothelial cell

ECM: Extracellular matrix

EDTA: Ethylenediaminetetraacetic acid

ePTFE: Expanded polytetra fluoroethylene

FBS: Fetal bovine serum

GPC: Gel permeation chromatography

MASMC: Mouse aortic smooth muscle cells

MMP: Matrix metalloproteinases

MMP-9KO: MMP-9 transgenic Knock Out

Mw: Molecular weight

PBS: Phosphate buffered saline

PCL: Poly e-caprolactone

PGA: Poly glycolic acid

PI: Propidium iodide

PLA: Poly lactic acid

PLGA: Poly D, L-lactic-glycolic acid co-polymer

PTCA: Percutaneous transluminal coronary angioplasty

rRNA: Ribosomal RNA

RRX: Rhodamine Red X

SEM: Scanning electron microscope

SMC: Smooth muscle cells

T: Annealing temperature

TCA: Trichloro acetic acid

TCPS: Tissue culture plates

TIMPs: Tissue inhibitor of MMPs

3D: Three-dimensional

2D: Two-dimensional

VASMC: Vascular aortic smooth muscle cell

WT: Wild Type

XPS: X-ray photon microscopy

ϕ: Composition

ϕ_{PCL}: PCL mass fraction

SUMMARY

The role of matrix metalloproteinases (MMP)-9 and processing condition of biodegradable polymer scaffold has been investigated to optimize engineering vascular constructs. For a small diameter vascular construct, uniform 10 μm thickness of high porous scaffolds were developed using a computer-controlled knife coater and exploiting phase transition properties of salts. The comparative study of fast vs. slow degrading three-dimensional scaffolds using a fast degrading poly D, L-lactic-glycolic acid co-polymer (PLGA) and a slow degrading poly e-caprolactone (PCL) indicated that fast degradation negatively affects cell viability and migration into the scaffold *in vitro* and *in vivo*, which is likely due to the fast polymer degradation mediated acidification of the local environment. MMP-9 was crucial for collagen remodeling process by smooth muscle cells (SMC). MMP-9 deficiency dramatically decreased inflammatory cell invasion as well as capillary formation within the scaffolds implanted *in vivo*. This study reports that the angiogenic response developed within the scaffolds *in vivo* was related to the presence of inflammatory response. Combinatorial polymer libraries fabricated from blended PLGA and PCL and processed at gradient annealing temperatures were utilized to investigate polymeric interactions with SMC. Surface roughness was also found to correlate with SMC adhesion. SMC gathering, proliferation, and protein production were highest in regions that exhibited increased surface roughness, reduced hardness, and decreased crystallinity of the PCL-rich phases. This study revealed a previously unknown processing temperature and blending compositions for two well-known polymers which optimized SMC interactions.

CHAPTER 1

Introduction

1.1 Overview

World Health Organization projections suggest that coronary artery disease (CAD) will remain the largest element of the global disease burden, reflecting the aging of the population. Current options for the management of CAD have their limitations, thus confirming the appropriateness of continuing the search for improved therapies to reverse the disease process and reduce the global burden (Sleight, 2003).

There are currently two main vascular surgical treatments for CAD: coronary artery bypass graft surgery (CABG) and percutaneous transluminal coronary angioplasty (PTCA) with or without stenting. For some patients, PTCA is a less traumatic and less expensive alternative to bypass surgery. However, in about 40 percent of patients treated by PTCA, the dilated segment of the artery narrows again within six months post-treatment. They may then require another PTCA or CABG surgery. Bypass grafting involves rerouting blood flow from a site proximal to the stenosis to a site distal to the ligation through an available vascular conduit. Due to effects of immunogenicity, thrombogenicity and compliance mismatch on the graft patency, the majority of bypass grafting procedures use autologous internal mammary arteries and/or the greater saphenous vein (Bergsma et al, 1998 and Cooley, 1998). Unfortunately, due to donor site disease or unavailability in the case of repeat surgery, these grafts are not always available. In those situations, other autologous arteries or veins such as the splenic and radial arteries or the basilic and cephalic veins (Acar et al, 1993) must be considered.

When these alternatives are unavailable, polymeric substitutes have been employed, however, anastomotic occlusions may be a problem (Weyand et al, 1999). Alternative approaches initially centered on the use of allografts and xenografts. Allografts consist of gluteraldehyde or cryopreserved greater saphenous veins or umbilical veins. Unfortunately, these grafts have one-year patency rates lower than 50% (Ochsner et al, 1984 and Canver, 1995). Studies investigating gluteraldehyde fixed xenografts have shown short-term patency rates of less than 20% (Mitchell et al, 1993). This has led to the investigation of biodegradable polymers for tissue-engineered substitutes, which can synchronize degradation time with the replacement by natural tissue production from autologous cells. Creating an autologous tissue construct for a suitable vascular graft has been considered as one of the potential ideal compensative methods. Finally, tissue-engineering applications have begun to create physiological models of human tissue *in vitro* (Griffith, 2002).

Vascular remodeling, defined as any enduring change in the size and/or composition of an adult blood vessel, allows adaptation and repair. Physiological and pathological vascular remodeling entails degradation and reorganization of the extracellular matrix (ECM) scaffold of the vessel wall, explaining the recent interest in the potential participation of specialized enzymes, called matrix metalloproteinases (MMPs). Soluble factors, cell-cell, and cell-matrix interactions finely tune MMP expression and activation spatially and temporally. The action of MMPs can evade normal control and push remodeling over the edge (Galis, 2002). A thorough understanding of the control and consequences of MMP actions may provide a new way to manipulate vascular remodeling.

This short review will first cover the methods for tissue engineering vascular equivalents. The second section will discuss the current knowledge regarding the application of biodegradable polymers as biomaterials for vascular constructs. The final section will review the role of MMPs in vascular biology and especially the process of vascular remodeling.

1.2 Tissue Engineered Vascular Equivalents

The low patency rates for polymeric or fixed tissues have led to the investigation of tissue engineering approaches to provide viable alternatives for graft materials. The focus has been on four major areas: a) Decellularization and recellularization of xenogenic tissues; b) Rolled sheets of arterial components (i.e. smooth muscle cells (SMC), fibroblasts and the cell synthesized extracellular matrix); c) Contracted collagen gels; and d) Cell seeding on non-degradable and biodegradable polymer scaffolds.

Decellularized tissue has been explored using either xenogenic arteries or small intestine submucosa. Human saphenous vein SMC have been shown to grow on decellularized porcine aortas (Bader et al, 2000 and Teebken et al, 2000). Human SMCs took two to three weeks for complete reseeding and were biocompatible, allowing for implantation and subsequent remodeling *in vivo*. Use of the small intestine submucosa allows for a plentiful supply of material and provides appropriate mechanical properties but depends on the anticoagulation method used to overcome the thrombogenicity of this material (Lantz et al, 1993). More work is necessary to determine whether these methods will be suitable for long-term treatment.

L'Heureux and his coworkers (1998) pioneered the use of rolled sheets of SMCs and fibroblasts. Human umbilical vein derived SMCs and human dermal fibroblasts were grown to confluence in culture and treated with ascorbic acid to accelerate matrix deposition and cross-linking. The SMC sheet was placed around a tubular mandrel to produce the medial layer. Subsequently, the fibroblast sheet was placed around the SMC media to form an adventitial layer. After mechanical preconditioning for up to 56 days, these vessels showed superior mechanical strength. Endothelium was then seeded into the lumen to provide all three-vessel layers. Grafts into the femoral artery of miniature pigs showed patency for 28 days. The preliminary results of this study looked promising but in view of time efficiency, it took too long to get enough mechanical strength for manipulating the construct.

The use of SMC or fibroblast contracted collagen gels has also been investigated. This process involves incubated cells with soluble collagen, allowing the collagen to gel, entrapping the cells. Subsequently, the entrapped cells exert traction on the collagen causing the gel to compact. Unfortunately, early experiments resulted in insufficient burst strength. A novel method showing limited success was to increase the mechanical strength by using a high powered magnet to help the initial alignment of the collagen (Tranquillo et al, 1996). A second method investigated the role of integrins, where compaction was shown to be dependant on which integrin-binding domains were used (Ogle et al, 1999). A third technique involved the glycation of collagen, in effect cross-linking the collagen and thus increasing strength (Girton et al, 2000). Using mechanical stimulation of the cell seeded collagen gel to induce further remodeling (Seliktar et al, 2000 and 2003) showed enhanced material properties. However, it has been reported that the initial beneficial improvement of mechanical properties was ultimately lost, which can be explained by failure of native arteries, where the vascular pathology was associated with the inappropriate degradation of the ECM scaffold of the arteries by MMPs (Galis, 1999). It was found that mechanical conditioning of SMC-collagen constructs results in an overall increase in MMP production, and an increase in enzymatic activity.

Early attempts to develop bypass grafts engineered from synthetic materials focused on the use of non-degradable polymers, such as Dacron™ or expanded polytetra fluoroethylene (ePTFE). When replacing larger vessels of 6-100 mm in diameter, these grafts were very successful, but when used in the coronary system where diameters are 3-4 mm, thrombotic events rapidly closed them off. The next step, perhaps the beginning of tissue engineering as applied to the cardiovascular system, was the development of endothelial cell (EC)-seeded synthetic grafts, which was started in the mid 1970s. The major limitation of the earlier grafts was the thrombogenic blood-contacting surface. The thrombogenic surface is removed by coating EC onto the synthetic surfaces (Weinberg and Bell, 1986). To optimize EC-binding, various approaches were taken (Nerem, 2001). Impregnating bioactive molecules such as FGF-1, heparin and fibronectin into high-density porous polyethylene and ePTFE was shown to enhance endothelial binding (Massia et al, 1991 and 1992; Chu et al, 1999; Can et al, 2000). These methods allow for continual mechanical support and favorable surfaces. Alternatively, combining techniques such as using contracted collagen as a medial layer with a polymeric outer tube, may provide both mechanical support and favorable surfaces (Matsuda et al, 1989). Another alternative is to use a less reactive surface. Implantation of Silastic tubing into the peritoneal cavity of rabbits accelerated tissue formation and showed increased graft patency along with contractile properties in response to stimuli and the apparent creation of elastic lamina (Campbell et al, 1999). These studies have shown possible ways to reduce the immunogenic and thrombogenic problems but do not solve the chronic problem caused by material erosion. The use of a non-biodegradable synthetic material would hinder the normal remodeling response of the vascular system. Vascular cells are not equipped to remodel ePTFE or Dacron™ in the same way they remodel collagen and elastin. Thus, the synthetic material becomes a physical barrier to long-term adaptation of the vessel. Similarly, the vasoactive component of the vessel would be completely lost with a synthetic graft, hence the move to application of biodegradable polymers to generate autologous tissue.

1.3 Biodegradable Polymers in Vascular Constructs

A wide variety of both hydrophobic and hydrophilic polymers have been developed (Griffith, 2000; Saltzman, 1996). Degradable polymers undergo extensive chain scission to form small soluble oligomers or monomers in the presence of body fluids or *in vitro* culture. This degradation may proceed by a biologically active process (e.g. enzymes present in body fluids) or by passive hydrolytic cleavage. Degradable polyesters based on lactide and glycolide monomers have been the workhorse synthetic polymers for scaffold construction (Griffith, 2002). Synthetic polyesters like poly-lactide, poly-glycolide and poly ε-caprolactone have been shown to degrade mainly by simple hydrolysis of the ester bonds into acidic monomers, which can be removed from the body by normal metabolic pathways. Other factors that affect degradation include hydrophobicity and molecular weight.

Previous efforts to solve the problem in engineered vascular grafts have led to the application of biodegradable polymers for *in vitro* generation of an autologous tissue construct. Autologous cell seeding within biodegradable poly-glycolic acid scaffolds allows for structural support while cell proliferation and matrix deposition compensates for the biodegradation of the scaffold (Niklason et al, 1999; Shum-Tim et al, 1999). SMCs within the scaffold were cultured for several weeks under pulsatile radial stresses (Niklason et al, 1999). During this development process, cells produced large amounts of matrix proteins concurrently with the degradation of the polymer scaffolding. The constructs were maintained in a culture medium that was supplemented with biochemicals known to promote synthesis of structural ECM proteins. Following eight weeks of *in vitro* maturation, the constructs were comprised mostly of vascular cells and ECM. After the maturation process, porcine ECs were seeded onto the lumen of the construct to form a confluent monolayer. The initial findings demonstrated that these constructs exhibited burst pressures greater than 2000 mmHg and desirable histological characteristics. The difficulty in using a cell-seeded polymeric scaffold approach for engineering vascular constructs is the determination of culture conditions. In this respect, the mechanical and biochemical signals experienced by the developing tissue should promote optimal construct development as the polymer degrades. In the case of cardiovascular tissue, the use of a dynamic culture is clearly warranted.

Although the biodegradable synthetic polymer-based approach brings much promise in terms of construct development, there are several issues that must still be addressed. Firstly, eight weeks of *in vitro* development are required for the construct to exhibit the desired characteristics. To increase efficiency, remodeling competence could be improved by shortening the natural tissue developing time. There is also some concern about the presence of residual polymer within the vessel wall causing an inflammatory response. The mechanical properties of the degradable polyesters are not always suitable for the construct due to their relative inflexibility and tendency to crumble upon degradation or to break in the mechanically dynamic culture conditions. Degradation also has to be controlled to synchronize remodeling in careful consideration of loss of mechanical strength.

1.4 MMPs in Vascular Remodeling

Vascular remodeling to create any enduring change in the size and/or composition of an adult blood vessel, not only allows blood vessels to adapt and heal normally but also underlines the pathogenesis of major cardiovascular diseases, including atherosclerosis and restenosis. Physiological and pathological vascular remodeling entails degradation and reorganization of the ECM scaffold of the vessel wall, explaining the recent interest in the potential participation of specialized enzymes, called matrix metalloproteinases (MMPs). (Galis 2002).

The current understanding of the role of MMPs in vascular remodeling has come from two sources: *in vitro* experimentation using vascular cells and *in vivo* models where MMPs have been identified within the vessel wall. *In vitro* experimentation has allowed control of MMP expression and activity, and investigation of subsequent effects upon cellular processes, such as cell migration and proliferation. *In vivo* models, on the other hand, have allowed for investigation of global effects of MMPs in physiologic and pathologic vascular remodeling.

Endothelial cells, the blood contacting cells lining the innermost layer of the arterial wall, have been shown to synthesize many MMPs as well as MMP inhibitors when cultured *in vitro* (Galis, 2002). Studies of cultured endothelial cells have all shown a basal expression of MMP-2, also known as gelatinase A. However, the expression of other MMPs was shown to depend on the source of the cells, the culture conditions, and treatments employed (Jackson et al, 1997).

SMCs, the major cell type in the artery wall, are important for the maintenance of vascular tone and mechanical properties. Cultured human SMCs have been found to constitutively express MMP-2 and have the capacity to express MMP-9 (also known as gelatinase B) under stimulation by cytokines (Galis et al, 1994). Migration of rat SMC through reconstituted basement membrane has been shown to be dependent on gelatinolytic activity (Pauly et al, 1994). Increasing endothelial production of nitric oxide decreased production of MMP-2 and MMP-9 by SMC and reduced SMC migratory ability (Gurjar et al, 1999), indicating a role for MMP in enabling regulation of SMC by endothelial cells. Another study has shown that over expression of tissue inhibitor of MMPs (TIMPs) in SMC affects SMC invasion, proliferation, and apoptosis (Baker et al, 1998). Furthermore, MMP production in SMC is affected through an $\alpha_v\beta_3$ integrin (Bendeck et al, 2000 and Kanda et al, 2000). MMP-9 appears to be involved not only in degradation, but also in the reorganization of a collagenous matrix, both facets being essential for the outcome of arterial remodeling (Galis and Johnson, 2002). The potential role of MMPs has been shown as effectors of SMC dependent remodeling in a murine model (Johnson and Galis, 2003). Knock-out of the MMP-2 and MMP-9 genes decreased SMC invasion *in vitro* and decreased formation of intimal hyperplasia *in vivo* by 81% and 65%, respectively. However, it was found that MMP-9, but not MMP-2, was necessary for the organization of collagen by SMCs. Likewise, MMP-9 deficiency resulted in a 50% reduction of SMC attachment to gelatin, indicating that SMCs may use MMP-9 as a communicator between the cell surface and the matrix. Understanding the specific roles of these MMPs, generally thought to be similar, could improve the design of therapeutic interventions aimed at controlling vascular remodeling.

Ex vivo and *in vivo* models of vascular remodeling have also supported the potential role of MMPs. Organ cultures of human saphenous veins have shown that MMP expression and activity are modulated by flow conditions (Mavromatis et al, 2000) and that the expression of TIMPs is increased during neointimal formation (Kranzhofer et al, 1999). In a mouse model of restenosis, we have shown that the time course of MMP-2 and MMP-9 expression is different, suggesting that these two MMPs may differentially affect lesion progression (Godin et al, 2000). Studies have also shown that MMP inhibitors can induce regression of vascular lesions (Cowan et al, 2000) and MMP-9 deficiency suppresses the development of abdominal aortic aneurysms in a mouse model (Pyo et al, 2000), suggesting inhibition as a possible treatment for these conditions. However, another study in mice has shown that while the inhibition of MMPs prevents cardiac rupture, it also impairs angiogenesis and ultimately leads to cardiac failure (Heymans et al, 1999). While the inhibition of MMPs might halt some of the pathological effects, it may also negatively impact necessary positive aspects of remodeling.

CHAPTER 2

Objectives

The experimental drivers of this study are development and fabrication of biodegradable polymer scaffolds and the investigation of the role of MMP-9 for improving remodeling of vascular tissue in these scaffolds. We hypothesized that MMP-9 is necessary for cell-matrix interaction and remodeling process for the function and survival of the scaffolds. Vascular aortic smooth muscle cell (VASMC) interaction with the scaffolds can be improved by optimizing the biodegradable polymer. Specifically, we investigated the following major topics.

2.1 Aim 1

Investigation of the rate-dependent degradation effect of biodegradable polymers on *in vitro* three-dimensional (3D) cell cultures on scaffolds and *in vivo* host response to implants. Little had been studied about the degradation rate-dependent acidic byproduct effect of the scaffold, even though the degradation products of biodegradable polymers were shown to be non-cytotoxic. We developed thin biodegradable polymer scaffolds that have a highly porous structure to simulate a small diameter vessel or multi-layered media structure of aortas or big diameter arteries. We specifically investigated the degradation rate-dependent effects of *in vitro* 3D growth of VASMC on the biodegradable scaffolds and *in vivo* cell invasion mediated angiogenesis necessary for the function and survival of the implants.

Thin biodegradable polymer scaffolds could be employed for tissue engineered vascular constructs. On the other hand, previous studies implied that the rate of degradation might affect cellular function including cell proliferation, connective tissue synthesis and host response, even though the degradation products were shown to not have cytotoxic effects (Babensee,1998; Lewandrowski,2000). However, little had been clearly proved about how the acidic local environment, which was degradation rate-dependent, affects the 3D cell culturing on the scaffold and the key consideration for *in vivo* scaffold implantation, namely, the *in vivo* host response such as inflammation and angiogenesis. For these purposes, we developed ten micron thick porous structured matrix scaffolds using various polymers: a fast degrading polymer (poly D,L-lactic-glycolic acid co-polymer, PLGA, 50:50) and a slow degrading polymer (poly ε-caprolactone, PCL). We investigated the impact of the polymer degradation rate on the viability of primary mouse aortic smooth muscle cells (MASMC) *in vitro* (on the scaffold) and *in vivo* (angiogenesis following cell invasion by implanting scaffolds in the backs of mice). This study would enable optimization of the degradation rate and the culture conditions for synchronization with the regeneration of vascular tissue.

- Live/dead assay with Flow Cytometry analysis and multi-photon microscopy imaging were used for two-dimensional depth-independent and 3D depth-dependent viability of MASMC respectively.
- Gel permeation chromatography (GPC) was used to measure the molecular weight change associated with *in vitro* and *in vivo* polymer degradation through interaction with cultured *in vitro* MASMC or implanting the scaffolds in the backs of mice.

- pH-sensitive fluorescent probes were used to determine the pH of the culture medium which was used for degradation of the polymer.
- Inflammatory cell-specific Geimsa and EC-specific CD31 (PECAM-1) staining were used to investigate *in vivo* cell invasion and subsequent angiogenesis into the scaffolds.

2.2 Aim 2

The role of MMP-9 in cell-matrix interaction for remodeling and the functional survival of the constructs containing biodegradable polymer scaffolds. We investigated the *in vitro* degradation properties of MMP-9 on collagen and biodegradable polymer scaffolds. The potential role of MMP-9 for collagen remodeling was investigated specifically upon biochemical stimulation. We investigated the role of MMP-9 in the *in vivo* cellular invasion into implanted scaffolds and subsequent angiogenesis.

It was previously reported that the initial improvement of mechanical properties in collagen and VSMC constructs would ultimately be lost. Dr. Galis hypothesized that the scaffold of collagen-based tissue constructs is degraded by specialized enzymes, called matrix metalloproteinases (MMPs). Recently Dr. Galis' lab demonstrated that cultured SMCs produce MMPs, and production of MMPs by the SMC-seeded collagen vascular constructs *in vitro* and showed that MMP-9 was involved not only in degradation, but also in reorganization of a collagenous matrix, both facets being essential for the outcome of arterial remodeling (Johnson and Galis, 2004). We proposed that biodegradable polymers can offer an alternative solution, so we can preserve the beneficial effect of MMPs, especially MMP-9, upon the organization of the tissue engineered construct, and improve the collagen production, deposition, and organization, namely remodeling modulated by MMP-9 especially upon ascorbic acid treatment. Furthermore, we investigated the role of MMP-9 *in vivo.* Specifically, we implanted the biodegradable scaffold in the backs of MMP-9 transgenic Knock Out (MMP-9KO) and Wild Type (WT) mice and observed inflammatory cell invasion into the biodegradable polymer scaffold following angiogenesis using a newly developed fluorescence microangiography method. In order to assess the roles of MMP-9, we performed the following experiments:

- Real time- RT PCR was used to measure collagen mRNA production.
- 3H-Proline incorporation assay was used to measure collagen protein accumulation to investigate degradation properties of MMP-9.
- Gel permeation chromatography (GPC) was used to investigate the effect of MMP-9 on the *in vitro* or *in vivo* degradation of biodegradable scaffolds.
- A novel quantitative assay using FITC labeled collagen was applied to investigate the effect of ascorbic acid associated with MMP-9 on collagen assembly (Johnson and Galis, 2003).
- Inflammatory cell-specific Geimsa staining was used for investigating the effect of MMP-9 *in vivo* on inflammatory cell invasion into the implanted scaffolds.
- Newly developed fluorescence microangiography with multi-photon microscopic imaging and quantitative xylene tissue extraction method was applied to examine MMP-9 influence on in vivo formation of angiogenesis and perfusion.

2.3 Aim 3

Optimization of composition and fabrication conditions for blending two biodegradable polymers that enhance properties of affected MASMC using combinatorial biosurface chips. We developed a *poly lactic-co-glycolic acid* (PLGA) and *poly ε-caprolactone* (PCL) blended combinatorial surface chip based on concentration and annealing temperature gradients. Using these combinatorial chips, we hypothesized that the phase separation mediated polymer properties by determining specific concentration and annealing temperature that could determine improved MASMC interactions.

A "combinatorial biosurface chip" technology has been developed for high-throughput assays of the effects of polymer surface chemistry and structure on cell function. This technology allows rapid screening of thousands of surfaces in order to design novel biomaterials or scope out variables prior to detailed culturing experiments, because libraries containing hundreds to thousands of distinct chemistries, microstructures, and roughness are prepared using composition spread and temperature gradient techniques (Meredith, 2003). In terms of controlling degradation rate and getting possible synergistic effects of combination, we decided to blend PLGA and PCL, and thus developed new combinatorial chips comprised of PLGA and PCL. MASMC population assays on the chips indicated that specific surface structures and properties could be regulated to enhance MASMC interaction. Therefore, we investigated the area-dependent variation of surface microstructure using various surface analysis techniques. Also, we tested cell adhesion, cell viability, and cell proliferation to verify which of the cell properties were affected by area-dependent property and caused the increase in cell populations in certain areas. Then, we measured area-dependent changes of various surface properties such as roughness, composition, hardness, and crystallinity to investigate which surface properties strongly correlated with the enhancement of the verified cell properties. Finally, we tested the correlation between the determined optimal surface and cell properties with uniform individual samples that represented each specific surface property. We investigated protein-mediated cell interaction with the polymer surface, observing the change of area-dependent protein production. We conducted the following experiments with newly developed combinatorial chips with PCL and PLGA.

- Cyber-green nucleus staining was examined using fluorescence microscopy and phospho-image scanning were applied to determine cell coverage of the chips.
- BrdU incorporation and live/dead assay were used for cell proliferation and viability tests.
- Reflected and polarized microscopy were used for macroscopic reconstruction of the entire chip surface. Atomic force microscopy (AFM) was applied to measure the roughness and hardness of the surface.
- Differential scanning calorimeter (DSC) and X-ray Photon Microcopy (XPS) were used to measure the surface crystallinity and composition respectively.
- Radioisotope-labeled protein incorporation assay was applied for non-specific protein production assays.

CHAPTER 3

The Effect of Scaffold Degradation Rate on Three-Dimensional Cell Growth and Angiogenesis

Sung H-J, Meredith JC, Johnson C and Galis ZS. *Biomaterials*. 2004; [in press]

3.1 Abstract

Even though degradation products of biodegradable polymers are known to be largely non-cytotoxic, little detailed information is available regarding the degradation rate-dependent acidic byproduct effect of the scaffold. *In vitro* and *in vivo* scaffold degradation rate could be differentiated using a fast degrading polymer (e.g., poly D, L-lactic-glycolic acid co-polymer, PLGA, 50:50) and a slow degrading polymer (e.g., poly e-caprolactone, PCL). We applied a new method to develop uniform 10 μm thickness of high porous scaffolds using a computer-controlled knife coater with a motion stage and exploiting phase transition properties of a combination of salts and water in salt-leaching method. We then verified *in vitro* the effect of fast degradation by assessing the viability of primary mouse aortic smooth muscle cell (MASMC) cultured in the three-dimensional (3D) scaffolds. We found that cell viability was inversely related to degradation rate and was dependent on the depth from the seeding (upper) surface toward the lower surface. The pH measurement of culture medium using fluorescence probes showed time dependent decrease in pH in the PLGA scaffolds, corresponding to PLGA degradation, and closely related to cell viability. *In vivo* analysis of scaffolds implanted subcutaneously into the back of mice, showed significant differences in inflammation and cell invasion into PLGA vs. PCL. Importantly, these were correlated with the degree of the functional angiogenesis within the scaffolds. Again, PLGA scaffolds demonstrated less cell mobilization and less angiogenesis, further supporting the negative effect of the acidic environment created by the degradation of biocompatible polymers.

***Key words*:** Biodegradable polymer; degradation; cell viability; pH; inflammation; angiogenesis.

3.2 Introduction

Synthetic biodegradable polymers have been used extensively for scaffold fabrication in tissue engineering applications because they can enhance the properties of constructs specifically the mechanical properties, while allowing control of degradation. Good biocompatibility and possibility to processed into desired configurations add to their popularity. A desirable feature would be synchronization of polymer degradation with the replacement by natural tissue produced from cells. Therefore, the degradation properties of a scaffold are of crucial importance for biomaterial selection and design but also the long-term success of a tissue-engineered construct.

We have used in our study poly D, L-lactic-glycolic acid co-polymer (PLGA) and poly e-caprolactone (PCL), previously studied in respect to porosity, behavior in static and flow conditions, with temperature and cyclic loading (Athanasiou et al, 1998; Agrawal et al, 2000 and 1998; Thomson et al, 1996). Both polymers have been shown to degrade mainly by simple hydrolysis of the ester bond into acidic monomers, which can be removed from the body by normal metabolic pathways. Other factors that affect degradation include hydrophobicity (Lu et al, 2000) and molecular weight (Lu et al, 1999; Miller et al, 1977). The degradation of a block co-polymer such as PLGA is affected by the ratio of hydrophilic poly glycolic acid (PGA) to hydrophobic poly lactic acid (PLA). PCL that has higher molecular weight with higher hydrophobicity than PLGA will degrade more slowly. The biocompatibility of these polymers also has been demonstrated in biological applications (Zentner et al, 2001; Hasirci et al, 2001; Kweon et al, 2003; Rizzi et al, 2001) and the previous reports implied that the rate of degradation might affect cellular interaction including cell proliferation, tissue synthesis and host response (Babensee et al, 1998; Lewandrowski et al, 2000). However, details of the potential effects of the acidic byproducts on the 3D cell culture or upon in vivo host response remain understudied.

We are interested in developing small diameter tissue engineered vascular constructs and thus for the purpose of this study we developed 10 micron thick porous biodegradable scaffolds. We investigated polymer degradation and rate-dependent effects comparing a fast degrading polymer (PLGA, 50:50 ratio of PGA to PLA) and a slow degrading polymer (PCL). MASMCs were cultured *in vitro* on the scaffolds and we assessed cell viability and measured the degradation rate dependent pH change of culture medium. We also implanted the scaffolds *in vivo* and investigated in time their population by cells, especially by inflammatory cells. Interestingly, we found that the degree of inflammation was related to the level of vascularization of implants through angiogenesis.

3.3 Materials and Methods

Scaffold fabrication. We used salt leaching to develop a porous structure as follows. Poly DL-lactide-co-glycolide (PLGA; Sigma Aldrich, St Louis, MO) with a 50:50 ratio of PGA and PLA and a molecular weight range of 40,000-75,000 Da and poly ε-caprolactone (PCL; Sigma; Mw =114,000 Da) were dissolved by solvent casting from chloroform (Sigma). Salt crystals were generated by exploiting phase transition properties of a combination of salts and water. The salt size was controlled by ultra-sonication time and filter size in the final step and calculated by image analysis of Scanning Electron Microscope (SEM) at random 20 pores of each three samples of the both polymers. Computer-controlled knife coater with a motion stage (Meredith et al, 1997) was used to generate an average 10μm thick polymer matrix, at a constant velocity and angle.

MASMC culture and polymer seeding. SMCs were harvested from explanted aortas of wild-type mice as previously described (Galis et al, 2002). Cells were grown in DMEM (Cellgro, Herndon, VA) supplemented with 10% FBS (Sigma). SMC were seeded ($1x10^5$) onto polymer discs cut to fit into 24-well plates. Culture medium was changed twice weekly throughout the experiments. Discs were analyzed at 1, 7, 14, 21 and 28 days post-seeding.

Subdermal scaffold implantation in mice. The polymer discs were sandwiched between two nitrocellulose filters (Millipore, Boulder, CO) to block the non-specific tissue in-growth into the polymer. The discs were subcutaneously implanted in the back of wild type 129/SvEv mice. The discs were harvested at 7, 14, 21 and 28 days post implanting for analysis.

Polymer degradation assay. The polymer molecular weight distribution for the sample polymer discs was determined by gel permeation chromatography (GPC) (Perkin-Elmer, Wellesley, MA) equipped with a refractive index detector (Perkin-Elmer). The dried samples were dissolved in tetrahydrofuran at a concentration of 8 mg/ml and eluted through the column at a flow rate of 1 ml/min at 37 °C. Polystyrene standards (Polysciences, Warrington, PA) were used to obtain a primary calibration curve. All samples of the same polymer type were analyzed at a single run. Variability in the determination of the both polymer molecular weight by GPC for undegraded samples was about 1% relative standard deviation.

SMC viability test. For two dimensional viability tests, MASMCs were dissociated from the scaffolds using an enzyme solution consisting of 100U collagenase 1A (Sigma) and 250 μg trypsin (Sigma) and incubated at 37 °C for 1 hour (Grafe et al, 1994). Cell viability was determined by staining with 3 μM calcein (Molecular Probes Inc., Eugene, OR) and non-viable cells were visualized by staining with 20 μM propidium iodide (PI) (Sigma) followed by flow cytometric analysis (Becton Dickinson, San Jose, CA) (Park et al, 2000).

3D sectional cell viability through the thickness of the polymer (from the upper to lower surface) was measured using optical sectioning of 3 μm intervals with a multi-photon LSM510 microscope (Zeiss, Oberkochen, Germany) fitted with a NLO 800 nm laser. Staining of SMC with calcein, PI and Hoechst 33342 (Sigma) for nuclei counterstaining was performed without dissociation from the scaffold. At each optical section, the total cell number was counted as total blue stained (Hoechst) nuclei. The viable and dead cell number was counted as green (calcein) and red (PI) cells respectively. We defined cells that stained with both calcein and PI as dying cells. The viability was calculated as a percentage of green stained cells out of the total cell number. Average cell viability was calculated for three regions: top surface, inner layer, and bottom layer.

Scanning electron microscopy (SEM). The scaffolds were air-and vacuum-dried, and their surfaces were prepared for observation with the SEM at the beginning and end of the observation period. The polymer samples were gold coated using a sputter coater (Pelco sputter coater 91000) set at 20 mA for a total time of 120 s (coating thickness, approximately 40 nm). The specimens then were imaged with JSM-5300 SEM (JEOL, Peabody, MA) operated at 20 kV.

Measurement of pH with fluorescence probe. To determine the effect of degradation on the pH around the scaffolds, the polymer discs were incubated in phenol-red free DMEM at 37°C for 1, 7, 14, 21 and 28 days. To determine pH, 10μl of 10 μM fluorescein (Sigma) was incubated with 1ml culture medium for 10 min at 37°C (Haugland et al, 1999). Fluorescence was measured using a CytoFluor multi well plate reader (Perseptive Biosystems, Framingham, MA) set at 485 nm excitation and 530 nm emission. A standard curve was generated by adding either HCl or NaOH to the phenol-red free DMEM to give pH values in the range of 5-8, followed by the addition of the fluorescein and measurement in the CytoFluor.

In vivo host reaction to implanted scaffolds. Implanted PLGA or PCL discs were harvested at 7, 14 and 28 post-implantation. The harvested disc was frozen-embedded with O.C.T compound (Tissue-Tek®, Sakura Finetek, Torrance, CA) in liquid nitrogen and sectioned using a cryostat (Leica, Nussloch, Germany). All cell nuclei were counterstained using hematoxillin-eosin. For detection of inflammatory cells we performed Geimsa staining (Richard-Allan Scientific, Kalamazoo, MI) at 45 °C for 30 min and differentiated in 1% acetic acid solution. In Geimsa staining, the negatively charged phosphoric acid groups of DNA attract the purple polychromatic dyes. The blue basophilic granules are stained by the polychromatic cationic dyes. Cationic cellular components such as erythrocytes and eosinophilic granules are stained by red and pink anionic dyes.

In vivo angiogenesis. Immunohistochemical staining to identify vasculature was performed using the endothelial specific marker CD31 (PECAM-1) on sections of the frozen-embedded disc using rat anti-mouse PECAM-1 (Santa Cruz Biotechnology Inc., Santa Cruz, CA) followed by Rhodamine Red X (RRX)-labeled goat anti-rat IgG (Jackson ImmunoResearch Laboratories Inc, West Grove, PA). Nuclei counter staining was performed with Hoechst 33258 (Sigma) to identify the areas of cell invasion. As a measure of angiogenesis, red colored PECAM-1 positive areas were measured and normalized by the total cellular area determined by blue nuclear staining.

Statistical analysis. All data is shown as mean ± standard error. The paired student's t-test was used to determine significance and a *P* value less than 0.05 was considered significant.

3.4 Results

Scaffold fabrication. After preparing the polymer a disc, scanning electron microscopy (SEM) was used to verify the uniformity of the thickness and the pore size of each disc [Figure 1]. Changing the weight ratio of the salts to polymer controlled the scaffold porosity. The ratio of the salts to polymer was 4.4 to 1, thus the porosity was calculated to approximately 80% (Agrawal et al 2000). The maximum porosity was found to be 90%, as the 10 μm thickness thin polymer lost its mechanical strength at such high porosity (data not shown). The pore sized distributed to 8.2± 1.8 μm in PLGA and 9.8± 0.6 μm in PCL. They showed somewhat different size distribution because of viscosity, but overall pore size could be controlled less than 10 microns diameter.

Two- and three-dimensional cell viability test on the polymers. The two-dimensional (2D) viability of MASMC cultured on either type of polymers were compared against that of MASMC cultured in tissue culture plates (TCPS), for up to 28 days in culture. We found patterns of decreasing SMC viability on both polymers [Figure 2]. The 2D viability on PLGA was significantly lower than that on TCPS at 7, 21 and 28 days post-seeding. In comparison with PLGA, the viability on PCL was not significantly decreased compared to that on TCPS for the time investigated.

The 3D viability test showed that MASMCs cultured on the surface of the scaffolds migrated into the scaffold through the inter-connected porous structure [Figure 3(a)]. Overall, at later time points cell viability decreased from the upper towards the lower surface of the scaffold. A significant decrease in cell viability within the scaffold compared to the upper surface of PLGA was detected starting at 14 post-seeding [Figure 3(b)]. In comparison, the significant decrease in cell viability was detected only at 28 days for PCL.

In vitro polymer degradation. GPC data confirmed that the two polymers degraded at different rates [Figure 4(a)]. Initially, the measured molecular weight was 40,000±200 Da for PLGA, while it was 114,000 ± 350 Da for PCL. The molecular weight of PLGA had significantly decreased by 14 days (18%) and decreased to 56% ±1% ($p<0.01$) by 28 days. PCL degradation was slower, showing only a statistically significantly decrease at 21 days (33%) and 28 days (39% ±1%, $p<0.001$).

SEM micrographs illustrated the time-dependent morphological change of both polymer scaffolds [Figure 4(b)]. Significant morphological changes of PLGA could be seen at 14 days, with the disruption of internal structure changing the surface morphology. PCL showed relatively little change in morphology at 14 days. Huge disruption of inter-connected structure and changes in surface morphology was seen in PLGA at 28 days, while PCL scaffold structure appeared less affected.

Effects on pH. As polymer degradation leads to acidic byproducts, we investigated the potential effects on the pH surrounding the scaffolds. The pH measurements were performed in the absence of cells to eliminate potential changes caused by cell growth [Figure 4(c)]. In comparison with TCPS, the pH of medium with the PLGA discs was lower from 1 day through 28 days. PLGA degradation caused a significant decrease in pH by 7 days and continued decreasing to a final 0.5 pH units by 28 days. However, there was no significant decrease and difference of pH change between TCPS and PCL over the entire period investigated (28 days).

In vivo polymer degradation. *In vivo* degradation of PLGA or PCL discs implanted subdermally on mice was measured by GPC. The measured *in vivo* rates of degradation were found to be faster than those measured *in vitro* [Figure 4(d)]. The molecular weight of PLGA had decreased by 7 days and continued to decrease by 73.5% ± 6.5% ($p<0.05$) at 28 days. This degradation was significantly faster than *in vitro* degradation (56 ± 1% at 28 days, $p<0.001$). PCL degraded more slowly than PLGA *in vivo*, degradation reaching significance by 21 days at 46.2% ± 2.3% ($p<0.05$). The degradation of PCL *in vivo* was also faster than that *in vitro* after the same length of time (39 ± 1% at 28 days, $p<0.001$), supporting the notion that the degradation rate of polymers depends on the environment.

In vivo inflammatory cell invasion. We found that the cell density in the polymer regions remaining at 28 days was greater in the PCL compared to PLGA scaffolds [Figure 5(a)]. Taking into consideration the different degradation rates, the cell data was normalized to polymer area [n=3 for each time point] to obtain a measure of cell migration into the scaffold. We found that a significantly greater number of total cells migrated into PCL than PLGA at all time points, the increased acidic environment likely inhibiting cell migration. We also determined that migration of inflammatory cells followed a similar trend at 7 and 14 days. At longer time points, we did not find a statistical difference in the migration of inflammatory cell into the polymers, however at this time point quantification was less reliable due to significant polymer degradation.

In vivo angiogenesis. To measure the extent of angiogenesis within the implanted scaffolds, we detected the endothelial cell specific marker CD31 in histological sections of scaffold harvested at various times after implantation [Figure 5(b)]. We hypothesized that more *in vivo* cell invasion relating with inflammation [Figure 5(a)] would result in a greater angiogenic response. A higher density of CD31 positive cells was detected in the PCL than PLGA from 14 to 28 days. The CD31 positive area was normalized to total tissue area [n=3 for each time point] to determine the extent of angiogenesis. Significantly more angiogenesis was observed in PCL than PLGA scaffolds from 14 to 28 days, supporting the hypothesis that angiogenesis was related to increased invasion of scaffolds, specifically by inflammatory cells.

3.5 Figures and Legends

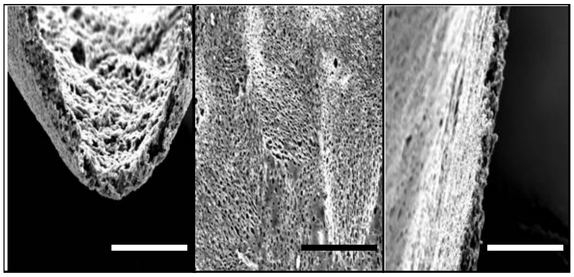

Figure 1. PLGA can be used to create thin porous scaffolds of uniform thickness. Morphology of a PLGA scaffold as visualized by scanning electron microscopy (SEM). Left and right pictures demonstrate the possibility to control the scaffold thickness (left: 15 µm, right: 10 µm). Center image illustrate a surface view. Pore size: < 10 µm. Porosity: approx. 80 %, Scale bars represent 50 µm.

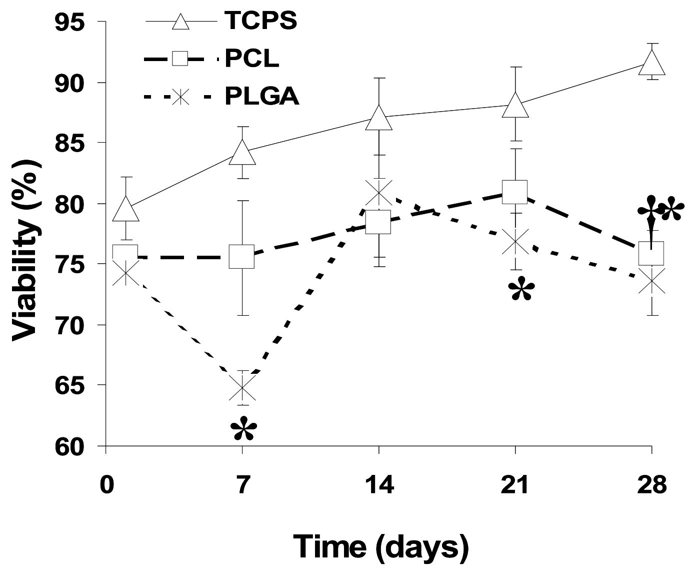

Figure 2. Detection of cell viability using primary cultured mouse aortic smooth muscle cells (MASMC). Two-dimensional viability was measured for cells cultured on PCL or PLGA scaffolds compared to that of cells maintained under regular cell culture conditions, on a tissue cell culture plastic surface (TCPS) for up to 28 days. The means obtained from 4 independent experiments ± SEM are shown. The viability was decreased at short time points on PLGA, then at later time points also on PCL. (*) $P < 0.05$ for PLGA vs. TCPS and (†) $P < 0.05$ for PCL vs. TCPS.

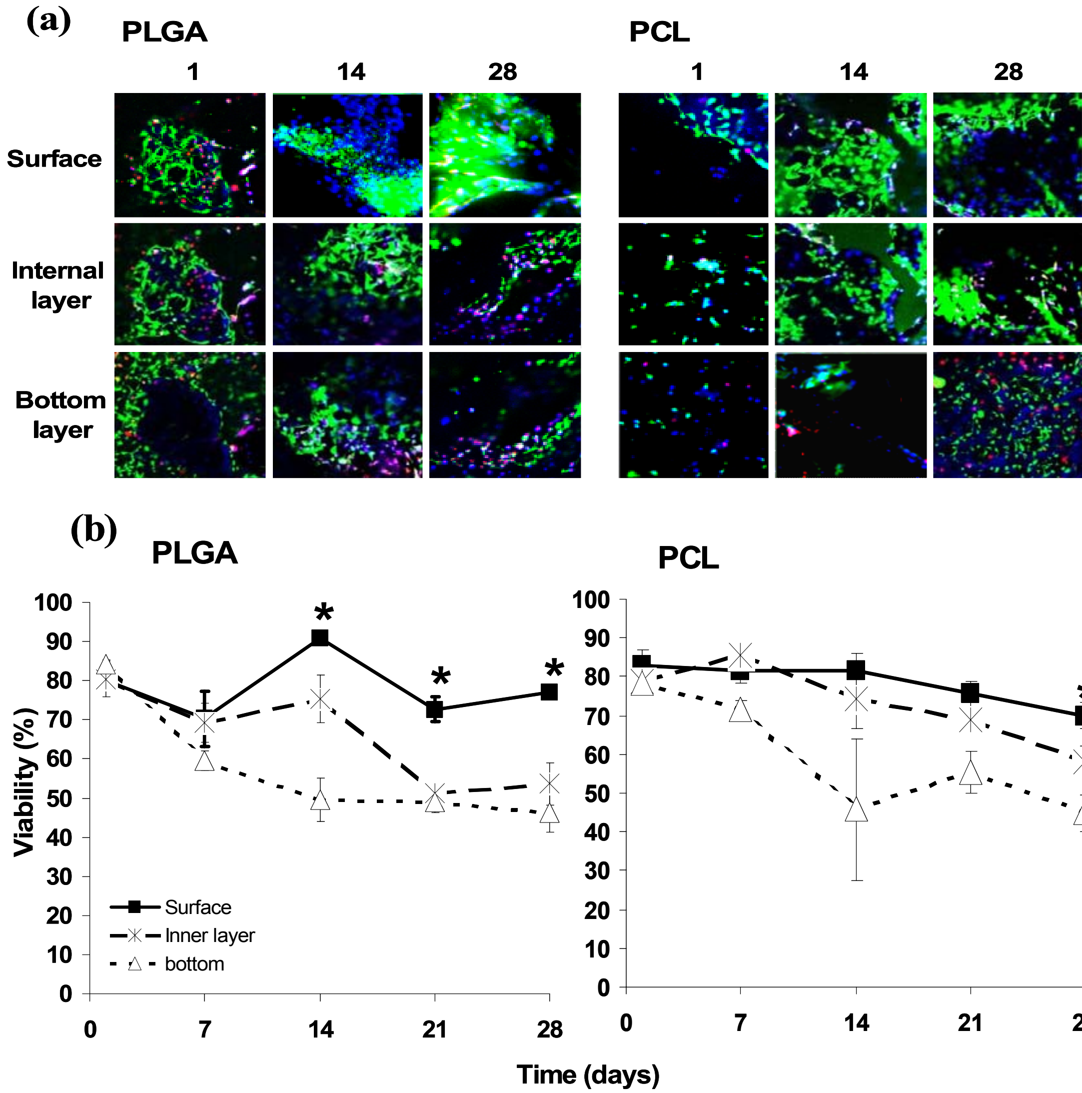

Figure 3. Cell viability within scaffolds (three dimensional, 3D) decreased with depth and as a function of time. Polymer discs cultured with MASMC for various length of time were analyzed by multi-photon microscopy using z-series at 3 micron interval optical sections. Top panels (a) illustrate cell viability in the three main regions (upper surface, middle region, bottom surface) after culture on PLGA (left) and PCL (right) for 1, 14, 28 days (viable cells are green, dead cells are red, all nuclei are blue) (b) Quantitative analysis of 3D viability in the three regions of PLGA (left) and PCL (right) scaffolds. The mean values obtained from 3 experiments ± SEM are shown. (*) $P < 0.05$ for surface vs. the other layers - internal and bottom layers.

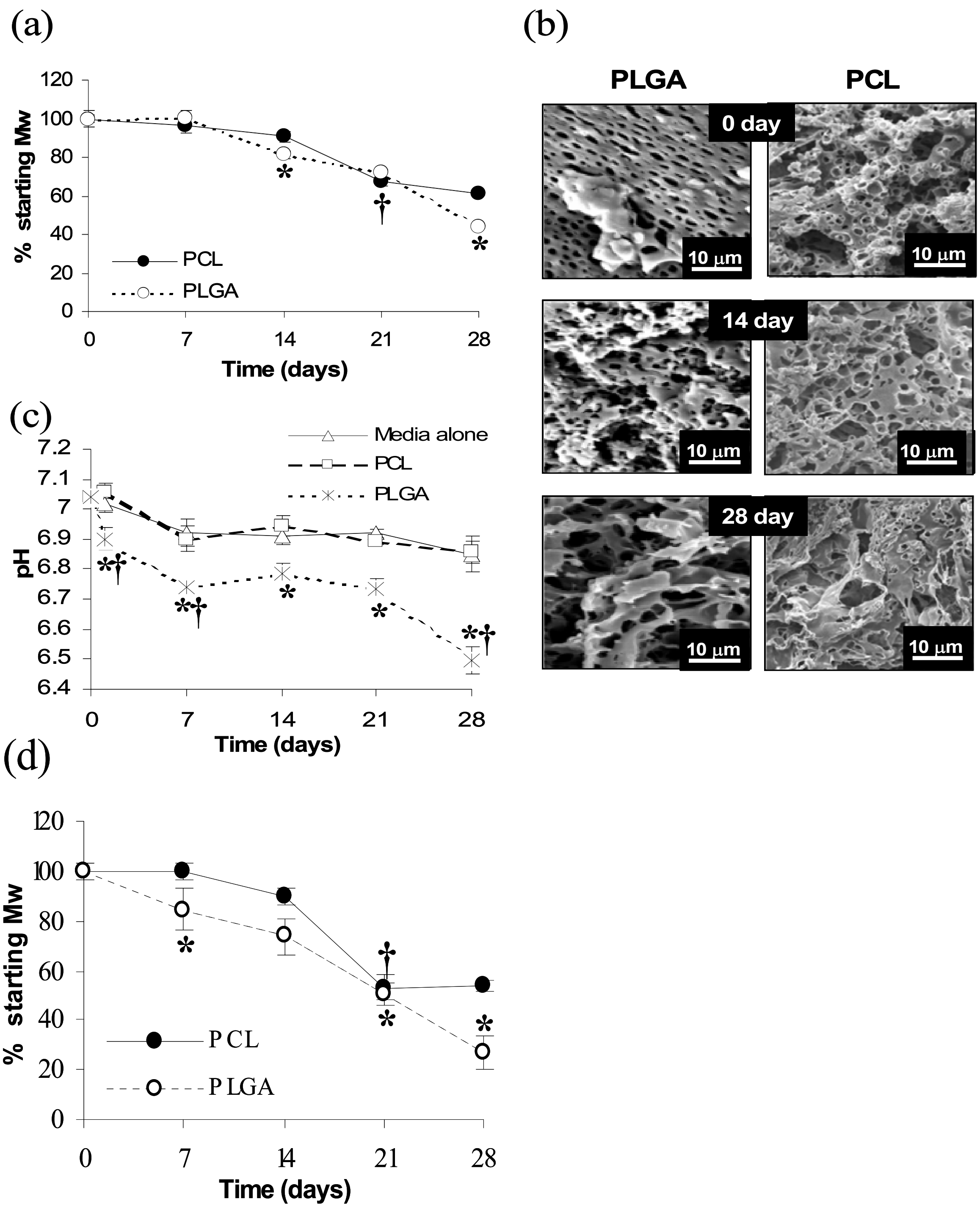

Figure 4. Characterization of PLGA and PCL scaffolds degradation *in vitro* and *in vivo*. (a) Measurement of *in vitro* degradation by GPC. Y-axis represents the % of starting molecular weight (Mw). Error bars represent SEM for n=3. (*) $P < 0.05$ for percent decrease from previous value for PLGA degradation and **(†)** $P < 0.05$ for percent decrease from previous value for PCL degradation. (b) Investigation of scaffold

morphology by SEM reveals effect of degradation at 14 and 28 days compared to day 0. (c) The environment pH changed as function of polymer and time, as measured using fluorescent probes. (Δ) Media minus scaffold (negative control), (ڨ) PCL and (x) PLGA. The mean values obtained from 4 experiments ± SEM are shown. (*) $P < 0.05$ for each polymer vs. control (culture medium alone) and (†**)** $P < 0.05$ for the value change compared to the previous value. (d) Degradation of polymer scaffolds was faster *in vivo,* measurement by GPC – compare to graph illustrated in (a). Y-axis represents the % of starting molecular weight (Mw). The mean values obtained from 3 experiments ± SEM are shown. (*) $P < 0.05$ represents PLGA value compared to value at previous time point and (†**)** $P < 0.05$ represents PCL value compared to previous time point for PCL.

(a)

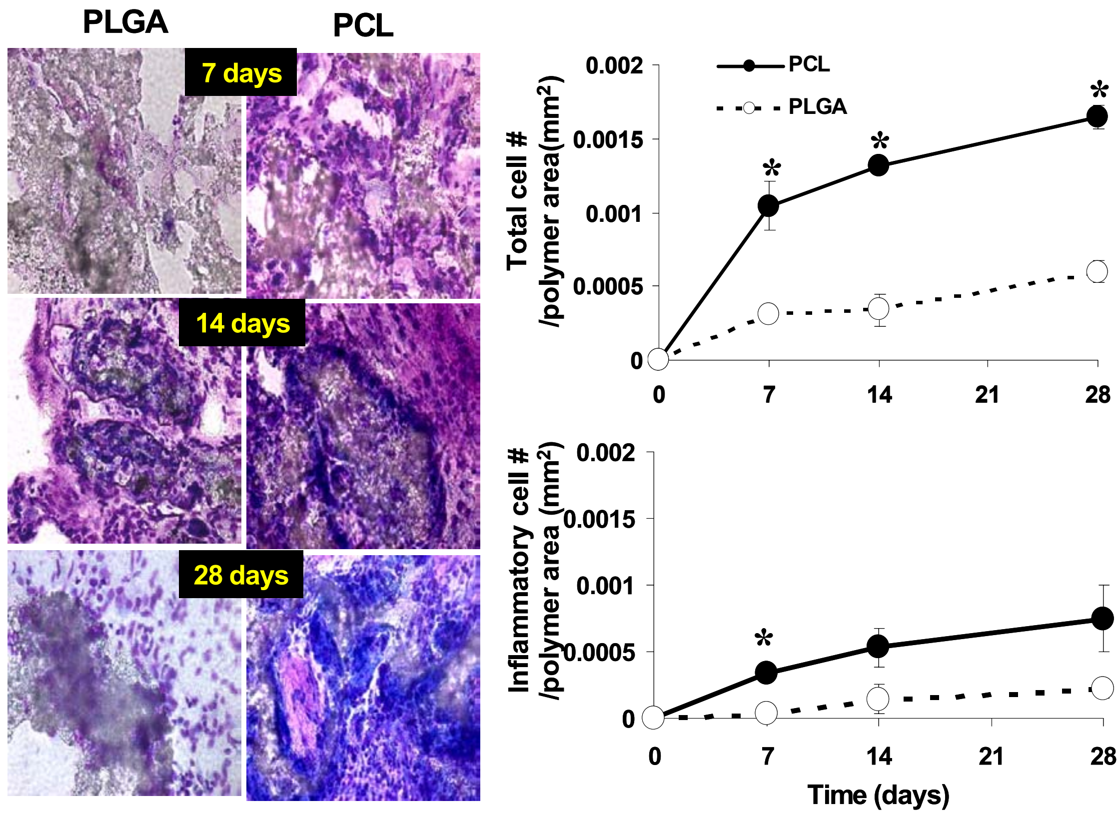
PLGA
PCL
7 days
14 days
28 days
PCL
PLGA
Total cell #
/polymer area(mm²)
0.002
0.0015
0.001
0.0005
0
0
7
14
21
28
*
*
*
Inflammatory cell #
/polymer area (mm²)
0.002
0.0015
0.001
0.0005
0
0
7
14
21
28
*
Time (days)

(b)

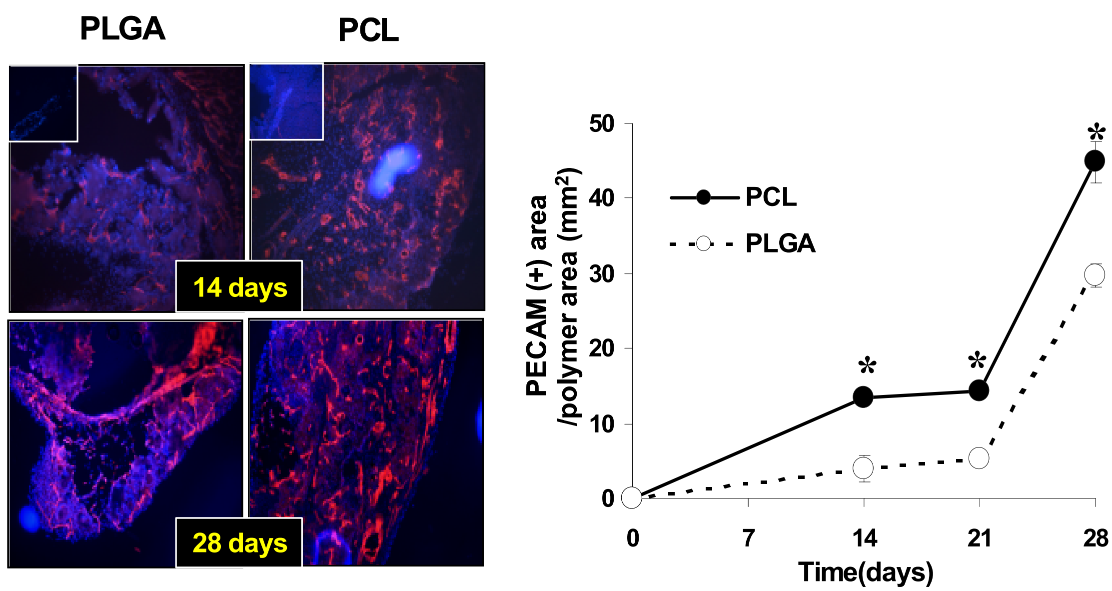
PLGA
PCL
14 days
28 days
PCL
PLGA
PECAM (+) area
/polymer area (mm²)
50
40
30
20
10
0
0
7
14
21
28
*
*
*
Time(days)

Figure 5. Analysis of cell population of biodegradable scaffolds PLGA (right panel) and PCL (left panel) implanted *in vivo* was determined initially (day 0) and at 14 and 28 days (frozen sections). (a) Presence of cells is indicated by the purple nuclear staining. Inflammatory cells are detected by Geimsa staining (blue and pink staining). Quantification of total cell density (right upper graph) and inflammatory cell density (right lower graph) indicated a significantly increased cell invasion into PCL vs. PLGA scaffolds implanted *in vivo*. (b) To determine the extent of angiogenesis, frozen sections were stained with an antibody against the endothelial marker CD31 (PECAM-1). Positive profiles were detected using red fluorescence. All nuclei were counterstained with Hoechst (blue). The data obtained for endothelial positive staining, considered to represent angiogenesis, normalized to polymer area for both PLGA and PCL, indicated a significantly increased vascularization of PCL scaffolds implanted *in vivo*. Error bars represent SEM for three separate implanted scaffolds (n=3). (*) $P < 0.05$ for PLGA vs. PCL.

3.6 Discussion

This study demonstrated the negative effect of fast degradation of scaffolds upon the *in vitro* viability of cultured primary SMCs. Analysis of scaffolds implanted into the back of mice, further supported this observation by showing less population with cells and angiogenesis within rapidly degrading scaffolds. We suggest that these effects were due at least partially to the increasingly acidic environment resulting from the degradation of PLGA vs. PCL. Use of dynamic flow would likely reduce the buildup of the acidic local pH of PLGA.

We also report a method to control the thickness of biodegradable scaffolds using a knife-edge coater with a computer-controlled motion stage at a constant velocity and angle. Pore size within the scaffold was controlled by the use of phase-transitional salts. For our particular application we created 10 μm scaffolds with pore of 8.2± 1.8 μm for PLGA and 9.8± 0.6 μm for PCL. Such scaffold will likely be useful to generate a highly porous 3D structure to optimize growth of vascular SMCs from aortic media (Ishii et al, 2001; Li et al, 2003).

We found that degradation of scaffolds made of either PLGA or PCL was faster *in vivo* than *in vitro*. Hydrolysis of PLA-PGA and PCL materials is influenced by the concentration of carboxylic acid end-groups, thus the degradation products of those materials may serve as catalysts for the reaction in static conditions, which likely accelerate degradation (Li et al, 1990; Therin et al, 1992). We also confirmed that more hydrophilic side chains and lower molecular weight of PLGA accelerated its degradation compared to PCL (Giunchedi et al, 2003). On the other hand, our study suggest that it is possible to accelerate the degradation of PCL, which although popular as a soft and hard-tissue compatible material had somewhat limited application because of its slow degradation kinetics. Various approaches have been previously employed to enhance its degradability, for example, PCL diol with acryloyl chloride (Kweon et al, 2003). However, degradation is also affected by the scaffold thickness and porosity. In our application, the faster than expected of PCL degradation was likely related to the fact that the PCL thin films had a greater surface area to volume ratio and thus a greater water uptake (Lu et al, 1999).

We found that the population with cells of scaffolds implanted *in vivo* was also dependent on the nature of the scaffold. Under similar conditions, the population of scaffolds with host's cells, specifically with inflammatory and endothelial cells, were found to be significantly lower in the PLGA compared to the PCL scaffolds, suggesting that the acidic pH and/or the rapid degradation of the scaffold prevented integration. Thus, we suggest that PCL may be more desirable for the survival of thin scaffolds implanted *in vivo*. Interestingly, the degree of inflammation seemed to be related to the degree of angiogenesis, further demonstrating the biocompatibility of degradation products (Perugini et a, 2003). Importantly, our results support the necessity of eliciting an appropriate host inflammatory responses in order to enhance the local recruitment of vasculature to tissue engineered constructs, essential for their integration as well as the long-tern survival and function.

Conclusion: We developed 3D biodegradable scaffolds using a new method to control the thickness using a knife-edge coater with a computer-controlled motion stage and the pore size using phase-transitional salts. The comparative study of fast vs. slow degrading 3D scaffolds indicated that fast degradation negatively affects cell viability and migration into the scaffold *in vitro* and *in vivo*. This effect is likely due to the significant acidification of the local environment due to the polymer degradation. We also report that the angiogenic response developed within the scaffolds implanted *in vivo* was related to the presence of inflammatory response. Our results should contribute to a better understanding of the cell-biodegradable scaffold interactions necessary to optimize the manufacturing and survival of tissue constructs.

CHAPTER 4

Matrix Metalloproteinase (MMP)-9 Facilitates Cell-Matrix Interactions for Function and Survival of Vascular Constructs

Sung H-J, Johnson CE, Magid R, Lessner SM, Drury DN and Galis ZS. *Tissue Eng*; [in review]

4.1 Abstract

Degradation of the extracellular matrix, facilitated by matrix metalloproteinases (MMPs), can lead to mechanical failure of vascular constructs, suggesting that MMP inhibition could improve survival of constructs. Therefore, we investigated the role of MMP-9 for *in vitro* collagen remodeling by smooth muscle cells (SMC), focusing on three major steps of production, degradation and organization. Since an adequate blood supply is essential for survival of tissue-engineered constructs, we also evaluated the influence of MMP-9 deficiency on vascularization of *in vivo* implant thin biodegradable polymer scaffolds. Using aortic smooth muscle cells (SMC) from wild type (WT) and MMP-9 genetically deficient (9KO) mice, we examined the role in MMP-9 on collagen mRNA expression and protein accumulation, both with and without ascorbic acid treatment. We measured effect upon collagen assembly using a fibrillogenesis assay. We investigated *in vivo* angiogenesis and cell invasion using fluorescence microangiography and histology. MMP-9 deficiency did not affect collagen mRNA production or polymer scaffold degradation, but collagen accumulation was greater in cultures of 9KO than in WT SMC. Both genetic deficiency and chemical inhibition of MMP-9 impaired collagen degradation. Ascorbic acid treatment enhanced collagen production by 9KO compared to WT SMC at 3 days, but by 7 days this effect was reversed, likely due to impairment of collagen fibril formation. MMP-9 deficiency dramatically decreased inflammatory cell invasion as well as capillary formation within biodegradable polymer scaffolds *in vivo*. Our data suggest that MMP-9 inhibition, by impairing collagen organization and angiogenesis, might have detrimental effects on the survival of vascular constructs.

Key words*:* matrix metalloproteinase-9; remodeling; collagen matrix; biodegradable polymer; inflammation; angiogenesis.

4.2 Introduction

We previously defined vascular remodeling as any enduring change in the size and/or composition of an adult blood vessel, allowing adaptation and repair (Galis et al, 2002). On the other hand, inappropriate remodeling, including its absence, underlies the pathogenesis of major cardiovascular diseases, such as atherosclerosis and restenosis. Physiological and pathological vascular remodeling entails degradation, production and reorganization of the extracellular matrix (ECM) of the vessel wall, explaining the recent interest in the potential participation of specialized enzymes, called matrix metalloproteinases (MMPs) (Galis et al, 2002). Mechanical stimulation of cell-seeded collagen gels induced further remodeling, resulting in enhanced mechanical properties (Seliktar et al, 2000 and 2003). However, the initial improvement of mechanical properties was ultimately lost, likely due tot the matrix degrading activity of MMPs secreted by the cells seeded in the constructs. This action seems analogous to mechanism leading to the mechanical failure of native arteries, where vascular pathologies have been associated with inappropriate degradation of the extracellular matrix scaffold of the arteries by MMPs (Galis, 1999).

MMP-9 (also known as gelatinase B) is necessary for the regulation of SMC replication and migration after arterial injury (Cho and Reidy, 2002; Johnson and Galis, 2004) and increased in perivascular inflammatory cell responses (Gurer et al, 2003; Ferroni P et al, 2003). Interestingly MMP-9 also appears to be involved not only in degradation, but also in reorganization of ECM (Galis et al, 2002), both facets being essential for the outcome of arterial remodeling (Mason et al, 1999). We also found that MMP-9 and MMP-2 considered to have similar functions actually differ in their actions related to SMCs interactions (Johnson and Galis, 2004). Monocytes cultured on collagen type I also released more MMP-9 than did cells plated directly on plastic (Wesley et al, 1998).

Angiogenesis is an essential component of a variety of physiological and pathological processes, and thus offers attractive opportunities to improve survival of implanted scaffolds. Angiogenesis triggered by tissue ischemia requires MMP-9, which appeared to be necessary for capillary branching and to be supplied by macrophage (Johnson and Sung et al, 2004), consistent with MMP participation in an inflammatory response (Silvestre et al, 2001).

Thus, we have decided to examine in more detail the value of using MMP-9 inhibition in order to preserve the integrity and function of tissue-engineered constructs. We first examined the hypothesis that biodegradable polymers may offer a solution for preserving the mechanical strength of scaffold matrix without necessity to inhibit the potential beneficial effect of MMPs, especially of MMP-9. However, addition of a synthetic biodegradable scaffold to the tissue engineered constructs involves the understanding of the effects of such materials upon the remodeling and integration of constructs in general and, particularly potential interference with the actions of the cell-secreted MMP-9. We investigated these issues using MMP-9 KO SMC and mice compared to the WT counterparts.

4.3 Materials and Methods

Scaffold fabrication. We used salt leaching to develop a porous structure as follows. Thin poly ε-caprolactone (PCL; Sigma; Mw =114,000 Da) films were solvent cast from chloroform (Sigma). Salt crystal size was controlled under 10µm diameter by exploiting phase transition properties of a combination of salts and water. A computer-controlled knife-edge coater with a motorized stage (Sung et al, 2004) was used to generate an average 10 µm thick polymer matrix, at a constant velocity and angle.

Mouse Aortic SMC (MASMC) isolation and culture. SMCs were harvested from explanted mouse aortas as previously described (Galis et al, 2002). We isolated cells from MMP-9 Knock-Out (KO) mouse strains with its strain matched wild-type counterparts, to allow for direct comparison. Cells were grown in DMEM (Cellgro, Herndon, VA) supplemented with 10% FBS (Sigma). SMC were seeded ($1x10^5$) onto PCL polymer discs cut to fit into 24-well plates or directly into 24-well culture plates. Culture medium was changed every day with or without 50 µM ascorbic acid (Sigma) throughout the experiments. Experimental analyses were performed at 3, 7, and 14 days post-seeding.

Subdermal scaffold implantation in mice. The PCL polymer discs were sandwiched between two nitrocellulose filters (Millipore, Boulder, CO) to constrain tissue growth into the polymer to two dimensions. The discs were subcutaneously implanted in the backs of MMP-9 KO and wild type 129/SvEv mice. The discs were harvested for analysis at 7 and 14 days post implantation.

Collagen mRNA production. Mouse collagen type 1 messenger RNA was quantified using quantitative real time reverse transcription PCR (SYBR Green method) on a LightCycler (Roche Applied Science, Indianapolis, IN). Total RNA was isolated using the RNeasy Kit (Qiagen, Valencia, CA) according to the manufacturer's instructions, including on-column DNA digestion (RNase-free DNase kit, Qiagen) to avoid genomic contamination. One microgram of RNA was reverse transcribed with Superscript II (Invitrogen, Carlsbad, CA). For quantification of collagen type 1, samples were run against a six-log standard curve of known plasmid concentrations (IMAGE clone 3466203) and normalized by 18 S rRNA level. Primers for normalization were QuantumRNA Classic II (Ambion, Austin, TX). The primers used for collagen type 1 amplification were 5'-GTCTGGTTTGGAGAGAGCATGA-3' (upper strand at 5) and 5'-CACAAGGGTGCTGTAGGTGAAG-3' (lower strand at 271). To ensure that only message and not potential genomic contamination was quantified, the primers were located in different exons, and the correct size of the product was verified through melting curve analysis after each run. Copy numbers were calculated for each sample by the instrument software using the second derivative maximum to determine the threshold fluorescence. Data were normalized against the static control for all time points prior to analysis.

Collagenous protein accumulation. The amount of total collagen protein was determined by radio labeling all synthesized proteins with L-[2,3-^{3}H]proline (PerkinElmer Life Sciences, Inc., Boston, MA) and by digesting collagenous proteins with collagenase (Sigma). MASMC were plated on the specimens in complete medium containing ^{3}H–proline, which was changed every 24 hrs. After incubation, the proteins were extracted following a previously described method (Suh et al, 2001). To account for differences in cell proliferation, the data were normalized to DNA content. We measured DNA content by SYBR green (Molecular probes, Eugene, Oregon) nuclear staining with fluorescence quantitation in a micro-well plate reader (Perseptive Biosystems, Framingham, MA).

Collagen degradation assay. Collagen type 1 degradation by MMP-9 was investigated in cultures of WT or MMP-9 KO MASMC using fluorescently conjugated bovine skin type 1 collagen (Molecular Probes, Eugene OR). Cells were seeded in 24-well plates with 10% FBS in DMEM for 24 hours. Fluorescein-conjugated type 1 collagen was treated with serum free DMEM for 3 days. In some experiments, cultures were treated with 50 μM ethylenediaminetetraacetic acid (EDTA, Gibco, Grand Island, NY) for 3 days to inhibit MMP activity. Conditioned media were treated with 1:15 TCA at 4 ^{o}C for 20 min, then centrifuged at 1,500 g for 5 min at 4 ^{o}C. The supernatants were transferred to new 24-well plates, and the fluorescence intensity of degraded collagen was measured in a micro-well plate reader (Perseptive Biosystems) at 495 nm excitation and 515 nm emission.

Polymer degradation assay. The polymer molecular weight distribution for the sample polymer discs was determined by gel permeation chromatography (GPC) (Perkin-Elmer, Wellesley, MA) equipped with a refractive index detector (Perkin-Elmer). The dried samples were dissolved in tetrahydrofuran at a concentration of 8 mg/ml and eluted through the column at a flow rate of 1 ml/min at 37 °C. Polystyrene standards (Polysciences, Warrington, PA) were used to obtain a primary calibration curve. All samples of the same polymer type were analyzed in a single run. Variability in the determination polymer molecular weights by GPC for undegraded samples was about 1% relative standard deviation.

Collagen fibrillogenesis assay. Investigation of the role of MMP-9 in collagen fibrillogenesis at the cell surface was performed using a previously described method with fluorescein-labeled collagen (Johnson and Galis, 2003).

In vivo host reaction to implanted scaffolds. Implanted PCL discs were harvested at 7 and 14 days post-implantation. The harvested discs were frozen-embedded with O.C.T compound (Tissue-Tek®, Sakura Finetek, Torrance, CA) in liquid nitrogen and sectioned using a cryostat (Leica, Nussloch, Germany). All cell nuclei were counterstained using hematoxylin. For detection of inflammatory cells, we performed Giemsa staining (Richard-Allan Scientific, Kalamazoo, MI) at 45 °C for 30 min, followed by differentiation in 1% acetic acid solution. In Giemsa staining, the cell nuclei stain purple, basophilic granules stain blue, and erythrocytes and eosinophilic granules stain pink to red.

In vivo angiogenesis. We used a method developed for functional fluorescence microangiography to investigate angiogenesis into the implanted scaffolds at 7 and 14 days post-implantation. Mice were sacrificed and perfused with 10ml heparinized saline (10 U/ml) injected through the left ventricle. Vessel capacity was determined using 0.1 micron fluorospheres (Molecular Probes) at 1:20 dilution in heparinized saline. The scaffolds were harvested after perfusion and analyzed either by fluorescence phosphor-imager (Amerhsam Bioscience, Piscataway, NJ) or by multi-photon fluorescence microscopy (Zeiss, Thornwood, NY). For imaging angiogenesis at the scaffold surface, the filter papers were detached, and the whole surface of the scaffolds was scanned to detect fluorescence-positive area. Detailed microvasculature could be visualized by multi-photon microscopy. For quantification of vessel capacity, the harvested scaffolds were incubated in xylenes at room temperature for 3 days to dissolve the perfused fluorospheres, and the relative fluorescence intensity was measured in a multi-well plate reader.

Statistical analysis. All data is shown as mean ± standard error with n=3 for each time point and each group. The paired student's t-test was used to determine significance and a *P* value less than 0.05 was considered significant.

4.4 Results

Effect of MMP-9 deficiency on type 1 collagen mRNA production, protein accumulation and degradation by SMC cultured on TCPS. Type 1 collagen mRNA production quantified by real time RT-PCR was not significantly different between WT and MMP-9 KO MAMSC on TCPS, for up to 14 days in culture. Collagen mRNA production increased up to 7 days, then decreased until 14 days in both WT and MMP-9 KO MASMC in culture [Figure 6(a)]. Collagen protein accumulation in WT cultures was significantly lower than in MMP-9 KO cultures at 7 and 14 days post-seeding, suggesting degradation of collagen with presence of MMP-9. In comparison with 7 days, the difference of collagen accumulation between WT and MMP-9 KO was reduced at 14 days [Figure 6(b)]. In experiments using fluorescently-conjugated type I collagen, MMP-9 KO MASMC generated significantly less degraded collagen than WT, indicating that type 1 collagen was degraded by MMP-9 [Figure 6(c)]. Inhibition of MMPs by EDTA, a non-specific MMP inhibitor, significantly reduced type 1 collagen degradation in both WT and MMP-9 KO MASMC, but there was no significant difference between WT and MMP-9 KO. The intensity of the degraded fluorescent conjugate collagen value by WT without EDTA, was 1056.7 ± 4.9. The intensity of degradation by WT with EDTA and by MMP-9 KO without EDTA was 844.3 ± 3.8 and 970.7 ± 2.1 respectively. The calculated type 1 collagen degradation by MMP-9 was about 40.5%. The concentration of EDTA was limited to 50 μM to avoid cytotoxicity (Kenney et al, 2003).

Polymer degradation and collagen accumulation in the scaffolds. Measurements of molecular weight distribution showed that there were no significant changes in polymer degradation between WT and MMP-9 KO mice, either in cultures of MASMC or after implantation in vivo up to 14 days [Figure 7(a), (b)]. This means that MMP-9 expressed either by MASMC or by other cells, in vivo did not degrade PCL scaffolds.

Collagen protein accumulation by WT MASMC in the scaffolds was significantly lower than that of MMP-9 KO MASMC at 7 and 14 days post-seeding, which also suggested the selective degradation of collagen by MMP-9 [Figure 7(c)]. Collagen accumulation increased rapidly between 0 and 7 days, then began to level off between 7 and 14 days in both WT and MMP-9 KO MASMC cultures, similar to the pattern observed on TCPS.

Ascorbic acid treatment and collagen assembly. To optimize the concentration of ascorbic acid, we evaluated type 1 collagen mRNA production at various concentrations. At 50 μM ascorbic acid, mRNA expression reached a maximum without any discernible cytotoxic effect (data not shown), in agreement with a previous study (Kurata and Hata, 1991; Davidson et al, 1997). Ascorbic acid treatment improved type 1 collagen mRNA production in both WT and MMP-9 KO MASMC. MMP-9 KO cells showed 625.7 ± 123 % improvement compared to untreated controls, which was significantly higher than the 189.9 ± 17.4 % increase in WT MASMC at 3 days. After 7 days of ascorbic acid treatment, however, collagen mRNA levels had fallen below those of untreated cells in both WT and MMP-9 KO cultures [Figure 8(a)]. Accumulation of collagen protein showed a different pattern from mRNA expression. Ascorbic acid treatment improved collagen protein accumulation 253 ± 6.4 % in MMP-9 KO MASMC compared to untreated controls, which was also significantly higher than the 223 ± 8.2 % increase in WT cells at 3 days. However, at 7 days WT improved to 306.6 ± 14.3 % of untreated controls, which was significantly higher than the 274.9 ± 8.8 % elevation in MMP-9 KO MASMC [Figure 8(b)]. To evaluate cell-mediated collagen assembly, we compared WT and MMP-9 KO MASMC in a collagen fibrillogenesis assay with and without ascorbic acid. To account for differences in cell proliferation, the data were normalized to cell number. WT MASMC demonstrated significantly more fibrillogenesis than MMP-9 KO, as we reported previously.[6] Ascorbic acid treatment improved collagen assembly significantly in both WT and MMP-9 KO, although WT showed significantly higher values than MMP-9 KO [Figure 8(c)]. Enhanced collagen assembly by WT MASMC might account for the observed difference in collagen accumulation compared to MMP-9 KO at 7 days.

In vivo host reaction to implanted scaffolds. To obtain a measure of cell migration into the scaffold, we found that the cell density in the PCL scaffolds remaining undegraded at 14 days was greater in the WT than in the MMP-9 KO mice [Figure 9(a)]. To account for differences in PCL scaffold degradation rates, cell numbers were normalized to polymer area. We found that MMP-9 deficiency significantly impaired the total cell invasion of PCL scaffolds implanted in vivo at all time points [Figure 9(b)]. Migration of inflammatory cells followed a similar trend at 7 and 14 days. We found that MMP-9 deficiency also significantly impaired inflammatory cell migration into PCL scaffolds in vivo at all time points [Figure 9(c)].

In vivo angiogenesis. To quantify the extent of angiogenesis over the entire surface of the implanted scaffolds, we measured the fluorescence-positive surface area occupied by injected microspheres in PCL scaffolds harvested at 7 and 14 days after implantation [Figure 10(a)]. Quantification by image analysis showed that a larger area of fluorescence due of perfusion of microspheres was detected in the WT than in the MMP-9 KO at 14 days [Figure 10(b)]. To visualize the angiogenic microvasculature within the implanted PCL scaffolds, we performed optical sectioning with multi photon microscope and 3-D image reconstruction of the perfused vessels in scaffolds harvested at 7 and 14 days after implantation [Figure 10(c)]. Microvasculature in scaffolds implanted into WT mice was more highly developed than in those implanted into MMP-9 KO mice at both 7 and 14 days. In WT mice, the microvasculature appeared to increase in extent and complexity from 7 to 14 days. Quantification of perfused vessel capacity using xylene extraction (Johnson and Sung et al, 2004) showed significantly more angiogenesis within PCL scaffolds harvested from WT mice than in those retrieved from MMP-9 KO mice at both 7 and 14 days. These results support the hypothesis that angiogenesis was related to increased inflammatory cell invasion of scaffolds [Figure 10(d)]. In summary, MMP-9 deficiency also impaired angiogenesis upon implantation of biodegradable scaffolds.

4.5 Figures and Legends

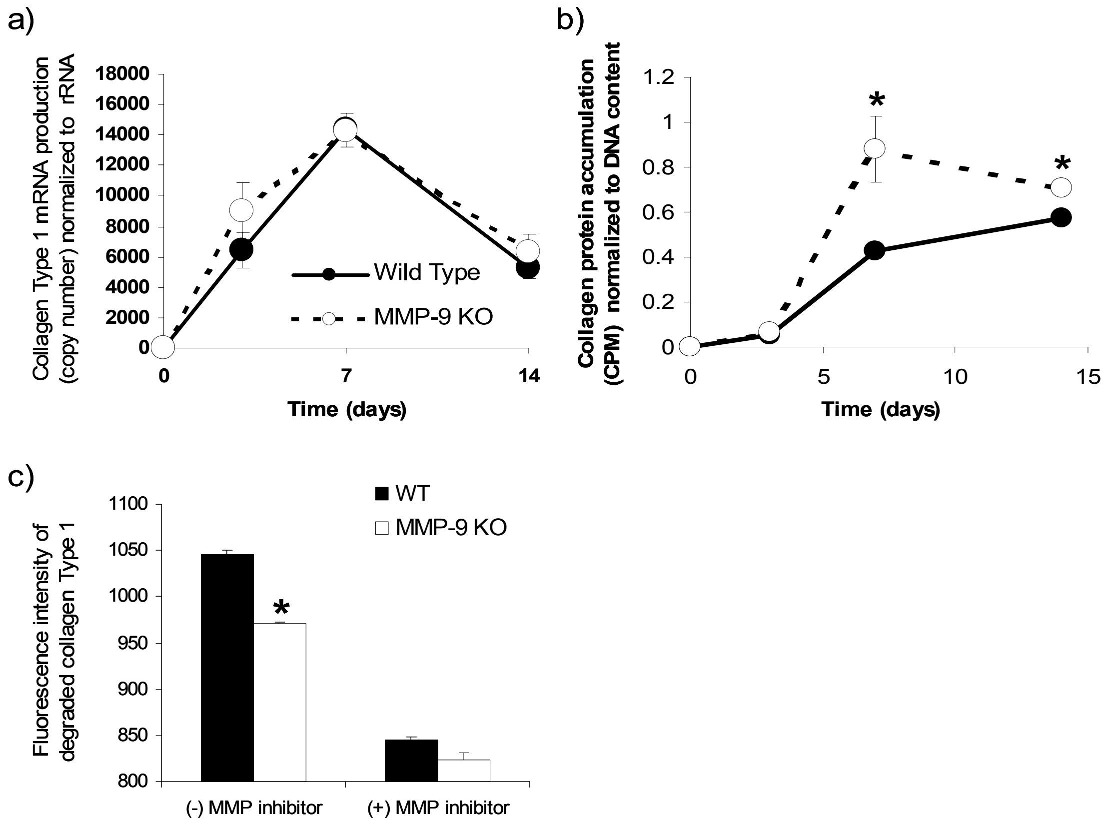

Figure 6. Effect of MMP-9 on collagen production and degradation on TCPS. (a) Collagen type 1 mRNA production was measured in cultures of WT and MMP-9 KO MAMSC using real time RT-PCR. The amplified copy number was normalized to 10^6 rRNA. (b) Collagen protein accumulation was measured in cultures of WT and MMP-9 KO MAMSC using a ^{3}H-proline incorporation assay. The CPM value was normalized to DNA content to account for differences in cell proliferation rates. (c) Degraded collagen in medium of WT and MMP-9 KO MAMSC was measured using fluorescently conjugated type 1 collagen from bovine skin. 50 μM EDTA was used as a nonspecific MMP inhibitor. Collagen mRNA production and protein accumulation analyses were performed up to 14 days. The means obtained from 3 independent experiments ± SEM are shown. (*) $P < 0.05$ for WT vs. MMP-9 KO.

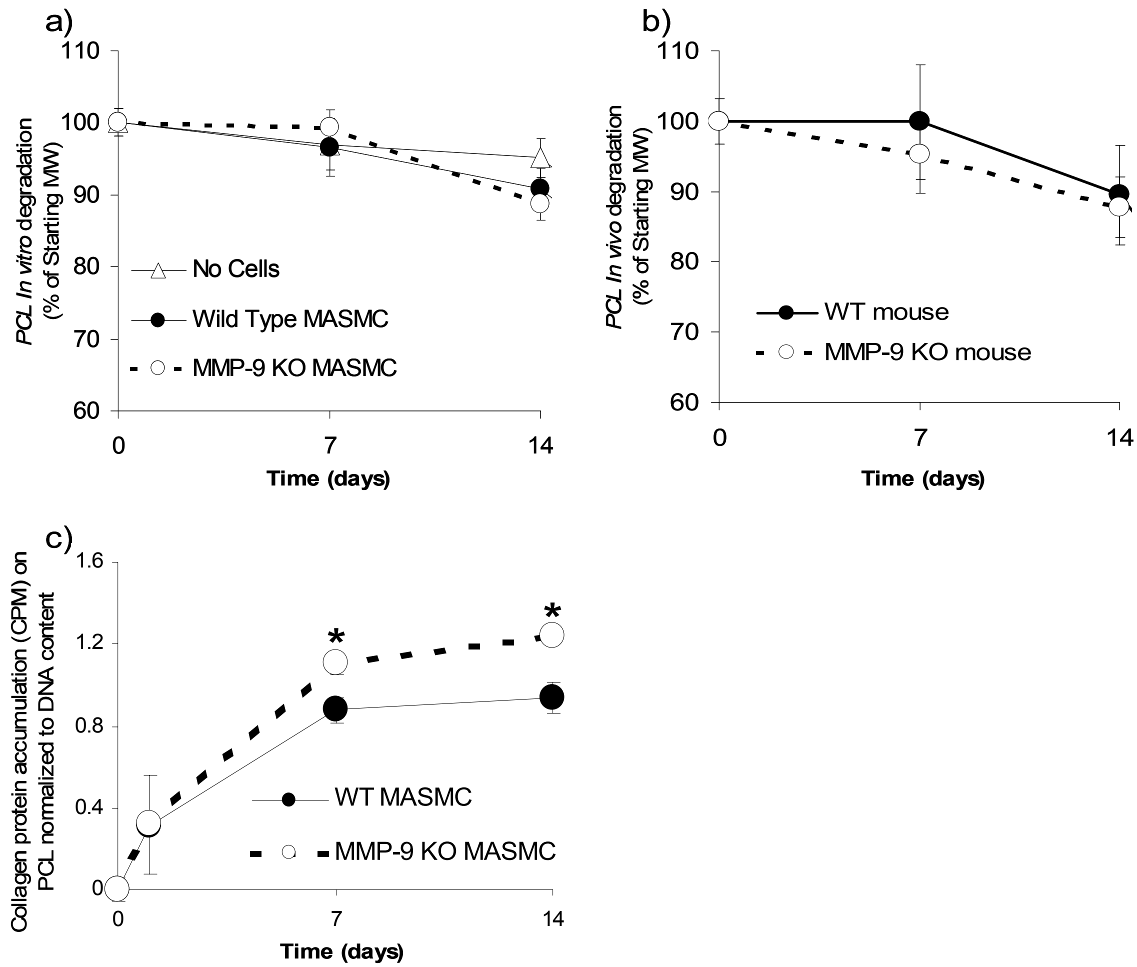

Figure 7. MMP-9 deficiency does not alter polymer degradation but increases collagen accumulation in PCL scaffolds. (a) *In vitro* degradation of the PCL scaffolds was measured in cultures of WT and MMP-9 KO MASMC or without cells as a control using GPC. (b) *In vivo* degradation of the PCL scaffolds was measured following subdermal implantation in WT or MMP-9 KO mice. (c) Collagen protein accumulation in the PCL scaffolds was measured in cultures of WT and MMP-9 KO MAMSC using a ^{3}H-proline incorporation assay. The radioactivity in CPM was normalized to DNA content to account for differences in cell proliferation rate. All the experiments were performed up to 14 days. The means obtained from 3 independent experiments ± SEM are shown. (*) $P < 0.05$ for WT vs. MMP-9 KO.

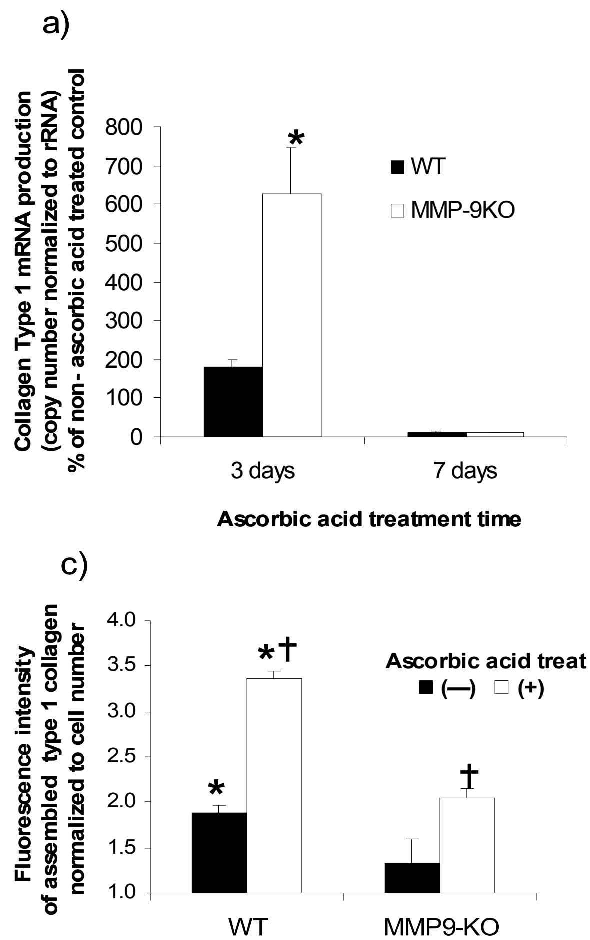

Figure 8. Effects of ascorbic acid treatment on collagen production and assembly. (a) Type 1 collagen mRNA production was measured in cultures of WT and MMP-9 KO MAMSC on TCPS with or without 50 μM ascorbic acid using real time RT-PCR. The amplified copy number was normalized to 10^6 rRNA. Data are presented as percentage of collagen production without ascorbic acid treatment. (b) Collagen protein accumulation was measured in cultures of WT and MMP-9 KO MAMSC on TCPS with or without ascorbic acid treatment using a ^{3}H-proline incorporation assay. The CPM value was normalized to DNA content to account for differences in cell proliferation rate. Data are presented as a percentage of the production without ascorbic acid treatment. (c) Collagen assembly was measured in cultures of WT and MMP-9 KO MAMSC on TCPS with and without ascorbic acid using a fibrillogenesis assay. Data were normalized to cell number. Collagen mRNA production and protein accumulation analyses were performed at 3 and 7 days. (*) $P < 0.05$ for WT vs. MMP-9 KO. (†) $P < 0.05$ vs. untreated controls.

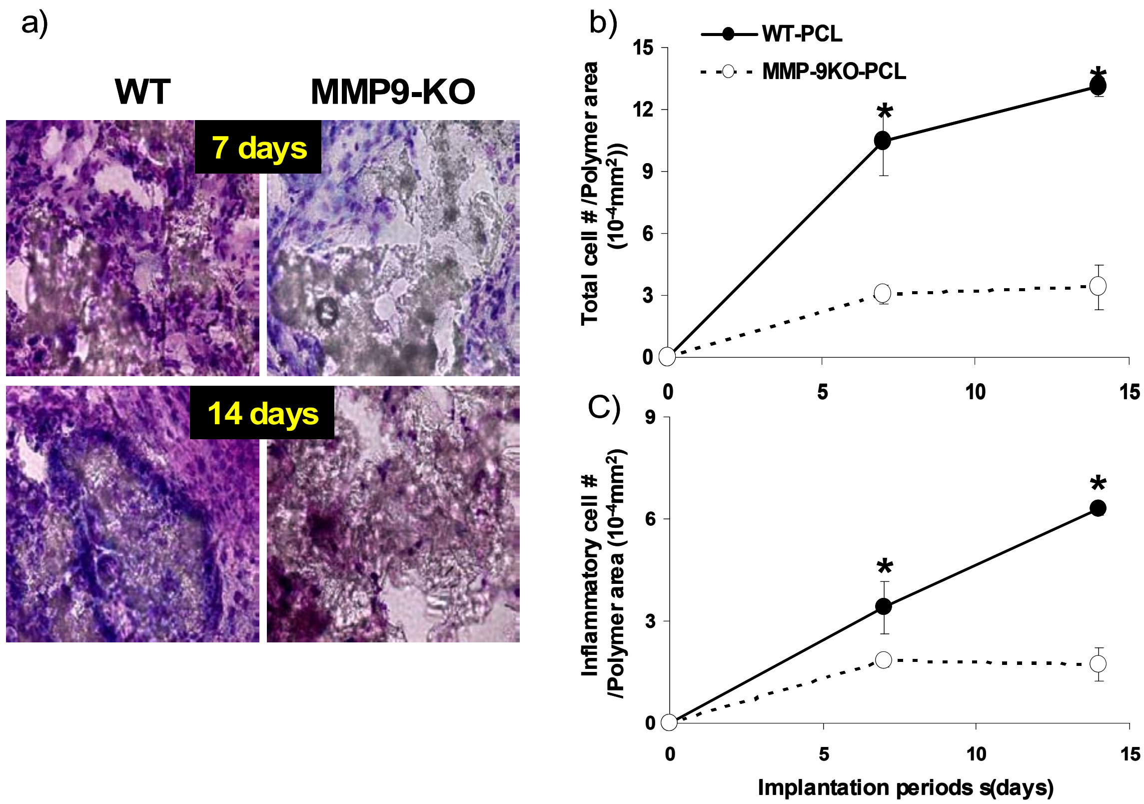

Figure 9. *In vivo* host reaction to implanted scaffolds. Analysis of cell infiltration into PCL scaffolds implanted in WT (left panel) and MMP-9 KO (right panel) mice was performed at 0, 7, and 14 days using frozen sections. (a) Presence of cells is indicated by the purple nuclear staining. Inflammatory cells are detected by Giemsa staining (blue and pink staining). (b) Quantification of total cell density and (c) inflammatory cell density indicated a significantly increased cell invasion into the PCL scaffolds implanted in WT vs. MMP-9 KO mice. Error bars represent SEM for three separate implanted scaffolds (n=3). (*) $P < 0.05$ for WT vs. MMP-9 KO.

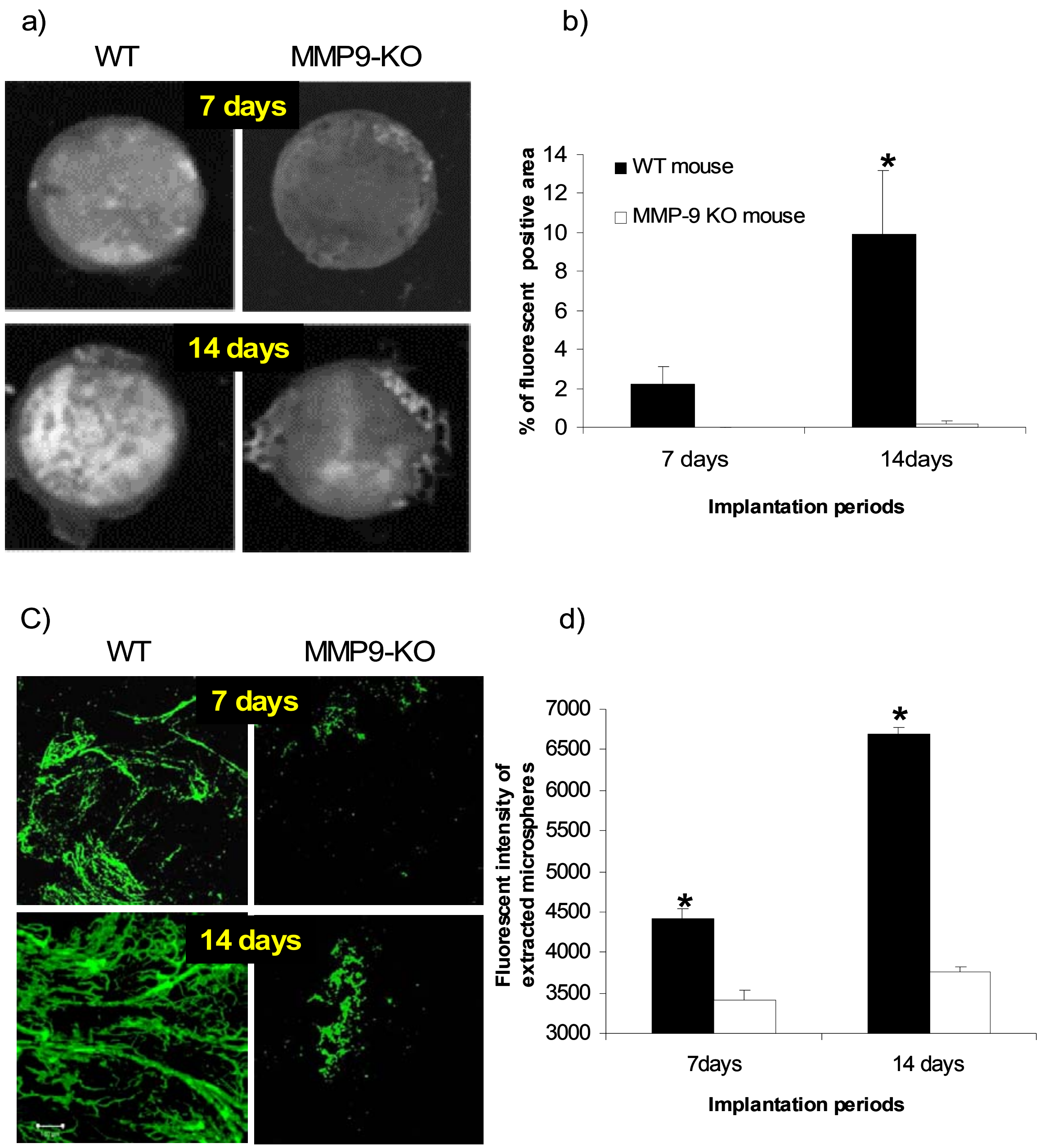

Figure 10. *In vivo* angiogenesis. Capillary formation in the PCL scaffolds implanted into WT (left panel) and MMP-9 KO (right panel) mice was assessed at 0, 7, and 14 days. (a) Fluorescence imaging was performed to determine the extent of angiogenesis on the surface of the scaffolds. (b) Angiogenesis was quantified by measuring the area of fluorescent bead perfusion into the scaffold (bright regions). (c) Multi-photon microscopic imaging was performed to visualize the capillary vasculature in the implanted scaffolds. (d) Functional vessel capacity was quantified by xylene extraction of perfused microspheres followed by fluorescence measurement. Error bars represent SEM for three separate implanted scaffolds (n=3). (*) $P < 0.05$ for WT vs. MMP-9 KO.

4.6 Discussion

Degradation of extracellular matrix, most likely by matrix metalloproteinases (MMPs), has been thought to lead to mechanical failure of vascular constructs, suggesting that MMP inhibition might improve survival of constructs. However, our results support the idea that MMP-9 contributes to improving collagen organization.

MMP-9 did not degrade PCL scaffolds *in vitro* or *in vitro,* but selectively degraded collagen in the scaffolds, which indicates that using biodegradable polymers as scaffolds can offer an alternative solution to prevent mechanical failure and preserve the beneficial effect of MMPs, especially MMP-9, upon the remodeling of collagen in the tissue engineered construct.

Without ascorbic acid treatment, MMP-9 deficiency did not affect collagen mRNA production, but resulted in increased net collagen accumulation by MMP-9 KO than by WT cells, possibly due to impaired collagen degradation.

In vitro collagen accumulation on TCPS at 14 days showed less difference between WT and MMP-9 KO than at 7 days, suggesting that improved collagen assembly such as fibrillogenesis in the presence of MMP-9 might affect long-term collagen accumulation. Upon treatment of ascorbic acid, collagen accumulation at 7 days in WT vs. MMP-9 KO, further supported the role of fibrillogenesis in collagen accumulation. Even though type 1 collagen mRNA expression was reduced by ascorbic acid treatment at 7 days, collagen protein accumulation was enhanced by ascorbic acid treatment at 7 days than at 3 days, possibly due to collagen accumulation. Improving MMP-9-mediated collagen assembly by ascorbic acid treatment could provide a method to enhance the remodeling process by synchronizing the degradation of the scaffold with growth of new ECM in tissue-engineered vascular constructs.

Proteolytic degradation of ECM components is an essential component of cell invasion and angiogenesis. During these processes, MMPs seem to be primarily responsible for much of the ECM degradation (Shian et al, 2003; Jia et al, 2000). We found that cell migration into biodegradable scaffolds implanted *in vivo* was also dependent on MMP-9 activity. The infiltration of PCL scaffolds with host cells, specifically inflammatory cells, was found to be significantly lower in MMP-9 KO mice compared to WT animals, suggesting that MMP-9 deficiency prevented integration into the host vasculature. Thus, we suggest that MMP-9 mediates several functions important for the survival of thin scaffolds implanted *in vivo*. Interestingly, the degree of inflammation seemed to be related to the degree of angiogenesis, further demonstrating the biocompatibility of degradation products (Gough et al, 2003; Corden et al, 2000). Importantly, our results support the role of MMP-9 in eliciting an appropriate host inflammatory response in order to enhance the local recruitment of vasculature to tissue engineered constructs, essential for their integration as well as their long-term survival and function.

CHAPTER 5

Combinatorial Screening of surface effects of biodegradable polymer blends for optimization of smooth muscle cell properties

Sung H-J, Su J, Berglund JD, Russ BV, Meredith JC and Galis ZS. Manuscript in preparation.

5.1 Abstract

Controlling cellular and physiological responses such as adhesion, proliferation, and migration is a highly desirable feature of engineered "bioactive" scaffolds. One important application would be the design of tissue engineered vascular grafts that regulate cell adhesion and growth. We utilized temperature-composition combinatorial polymer libraries to investigate the effect of surfaces of blended poly D,L-lactic-glycolic acid (PLGA) and poly ε-caprolactone (PCL) on murine smooth muscle cells (SMC). In this manner, SMCs were exposed to ~1000 distinguishable surfaces in a single experiment, allowing the discovery of optimal polymer compositions and processing conditions. SMC adhesion, aggregation, proliferation, and protein production were highest in regions with mid- to high-PCL concentrations and high annealing temperatures. These regions exhibited increased surface roughness, reduced hardness, and decreased crystallinity relative to other library regions. This study revealed a previously unknown processing temperature and blending compositions for two well-known polymers, which optimized SMC interactions.

Key words: tissue engineering; combinatorial polymer libraries; annealing temperature; composition; surface properties; SMC interaction.

5.2 Introduction

Synthetic biodegradable polymers have been used extensively for scaffold fabrication in tissue engineering applications because of their biocompatibility, degradation, and processability. However, actively controlling cellular responses such as adhesion, proliferation, and migration using "bioactive" surface features on the scaffolds (Meredith et al, 2003) remains an elusive goal that would greatly improve functionality. A fundamental challenge to this goal is the complexity introduced by combining materials science with biological science. Scaffold polymer surface chemical and physical (microstructural) properties can be adjusted in an almost infinite variety of combinations. When the complexity, uncertainty, and time-consuming aspects of cell culture and assays are added to the materials problem, conventional one-sample for one-measurement approaches become overwhelmed (Chicurel, 2001; Brocchini et al, 1998). The result is that only a select few material surface chemical-physical property combinations are explored in a typical study, leading to a large unexplored variable "space."

To address this challenge, a method for culturing cells on combinatorial polymer libraries prepared using composition spread and temperature gradient techniques was recently presented (Meredith et al, 2003; Meredith and Smith et al, 2000; Meredith and Aims, 2000). This approach allows hundreds to thousands of distinct chemistries and microstructure properties on a single sample that could be evaluated simultaneously for bioactivity towards a given cell line. The combinatorial method reduces discovery time by orders of magnitude via high-throughput analysis of cell-polymer interactions. Truly "bioactive" scaffolds can be identified quickly (as well as nonfunctional compositions), leaving more time and effort for a detailed examination of the mechanisms of the surface influence on cell behavior.

One technique for generating surface diversity that has not been explored significantly in tissue engineering is phase-separation of polymer mixtures. The "demixing" of two polymers generates unique combinations of surface chemistry, microstructure, nanostructure, and roughness by adjusting annealing temperature and composition (Meredith and Aims, 2000). To investigate possible synergistic surface structures in a blend, we prepared temperature (T)-composition (ϕ) libraries of poly(D,L-lactic-co-glycolic acid) (PLGA) and poly(ε-caprolactone (PCL)). While both polymers have been used extensively in implantable devices and tissue engineering, PLGA and PCL exhibit dissimilar properties including degradation rate, crystallinity, glass transition and melting temperatures, and mechanical characteristics (Supplemental Table 1) (Meredith and Aims, 2000; Lu and Peter et al, 2000; Lu and Garcia et al, 2000; Kweon et al, 2003; Schliecker et al, 2003; Lee et al 2003). The effect of their blending on surface properties and cell responses has not been studied. The effects of PLGA/PCL mixtures on primary aortic SMCs cultured on the libraries were investigated using multiple analysis techniques for cell adhesion, proliferation, aggregation, and protein production.

5.3 Materials and Methods

Preparation of combinatorial chips. PLGA block copolymer (50:50 ratio of PGA and PLA; Mw = 40,000-75,000 Da) and PCL (Mw =114,000 Da) were obtained from commercial suppliers (Sigma Aldrich, St Louis, MO). Combinatorial chips consisted of polymer films (22x 22 mm) coated onto clean glass slides. Annealing temperature (*T*,

^{o}C) and concentration (ϕ_{PCL}, mass fraction) gradients were generated along orthogonal directions. The composition gradient deposition process was applicable to a wide range of polymer blends and was described in detail elsewhere (Meredith et al, 2003; Meredith and Smith et al, 2000; Meredith and Aims, 2000). Briefly, a PCL solution in $CHCl_3$ (Sigma) was pumped into a mixing vial initially containing a PLGA solution while the mixture was withdrawn, resulting in an increase in PCL composition in the vial. A third automated syringe extracted the ϕ_{PCL} -gradient solution from the vial and deposited it as a thin stripe on the substrate. A knife-edge coater spread the liquid as a film orthogonal to the composition gradient. To explore a large processing T range, the ϕ_{PCL} -gradient films were annealed on a custom aluminum T-gradient heating stage for 2 hours, with the T-gradient orthogonal to the ϕ_{PCL} -gradient. A heat source and heat sink produced linear gradients ranging between adjustable end-point temperatures (Meredith et al, 2003; Meredith and Smith et al, 2000; Meredith and Aims, 2000). Each library explored a wide range in processing T ($50<T<120$)°C, and composition ($0.076 < \phi_{PCL} < 0.375$) mass fraction of PCL. Whole chip areas were divided to 9 regimes in the combination of $0.275 < \text{high } \phi_{PCL} < 0.375$, $0.176 < \text{mid } \phi_{PCL} < 0.275$ and $0.076 < \text{low } \phi_{PCL} < 0.176$ with $96.6 < \text{high } T < 120$ ^{o}C, $73.3 < \text{mid } T < 96.6$ ^{o}C and $50 < \text{low } T < 73.3$ ^{o}C for quantitative analysis.

Cell harvesting and culturing. The Institutional Animal Care and Use Committee of Emory University approved all animal protocols used in this study. SMC were harvested from explanted aortas of C57BL6/J wild-type (WT) mice (Jackson Laboratories, Bar Harbor, Maine) as previously described (Galis and Johnson et al, 2002). SMC cultured in DMEM (Cellgro, Herndon, VA) supplemented with 10% FBS

(Sigma), l-glutamine (Cellgro), and penicillin/streptomycin (Cellgro) were used in passages 3 through 8. Cells were tested and found to be >95% positive using a mouse anti-α-actin antibody (Sigma). SMC were seeded ($5x10^5$) onto combinatorial chips. Culture medium was changed twice weekly throughout the experiments.

Cell population and adhesion assay. Area-dependent SMC population measurements were performed on chips cultured up to 7 days. For cell adhesion assay, SMC were seeded on the chips and incubated for 8 hours. Medium was agitated to remove non-adhered cells. After culturing or agitating, SMC were fixed in 10% formalin and stained with SYBR™ green (Molecular Probes, Eugene, Oregon). Cell growth pattern, population and adhesion were observed using light and fluorescence microscope (Zeiss, Thornwood, NY), taking 10 × 10 grid of images over each cultured library. Localized area-dependent cell population or number was measured in the fluorescence images. The whole chip surface was scanned using fluorescence phosphor-imager (Amerhsam Bioscience, Piscataway, NJ).

To measure adhesion SMC population on the individual uniform scaffold, DNA content were measured by SYBR™ green (Molecular Probes, Eugene, Oregon) nuclear staining after agitating the non-adhered SMCs. Fluorescence intensity of SYBR™ green was measured for quantification in a micro-well plate reader (Perseptive Biosystems, Framingham, MA).

Cell viability and proliferation assay. SMC viability was determined by staining the combinatorial chips with 20 μM propidium iodide (PI) (Sigma) and SYBR™ green (Park et al, 2000) (Supplemental Figure 1). Cell proliferation was determined through BrdU incorporation and ^{3}H-thymidine uptake. 15μ M BrdU (BD Biosciences

Pharmingen, San Diego, CA) was added to SMC culture medium 12 hours before testing. SMCs were fixed with paraformaldehyde, then immunostained with primary rat anti-BrdU antibody (Abcam, Inc, Cambridge, MA) and secondary RRX goat anti–rat IgG antibody (Jackson ImmunoResearch Laboratories Inc, West Grove, PA). Nuclei counter staining was performed with Hoechst 33258 (Sigma) to visualize the total number of cells. Localized area-dependent nonviable cell or proliferating cell were observed using fluorescence microscope (Zeiss), taking 10 × 10 grid of images over each cultured library and counted in the fluorescence images (Lessner et al, 2002; Xi et al, 1997).

For the proliferation assay on the individual uniform scaffolds, 1μCi of ^{3}H-thymidine (PerkinElmer Life Sciences, Inc., Boston, MA) was added to SMC culture medium 24 hours before testing. After incubation, the cultured SMCs were rinsed with PBS twice, lysed and characterized for ^{3}H-thymidine incorporation (Zhang et al, 2003; Ruef et al, 1998).

Protein accumulation and production assay. To investigate localized medium protein accumulation on the combinatorial chips, 600 μCi of ^{35}S- methionine (PerkinElmer Life Sciences, Inc.) is treated every 24 hours up to 3 days without SMC seeding. To chase the localized protein production of SMC seeded on the combinatorial chips, 200 μCi of ^{35}S- methionine is treated every 24 hours up to 7 days (Tnasey, 2002; Rechinger et al, 2000). Methionine and cysteine depleted 10% FBS DMEM was used to treat ^{35}S- methionine. Medium protein accumulation and SMC protein production were visualized using phospho-fluorescence imager (Amerhsam Bioscience).

Polymer characterization.

Crossed-polar optical microscopy. Macroscopic reconstruction of entire chip surfaces were obtained by crossed polar optical microscopy using a BX51 Microscope System (Olympus, Melville, NY) to identify regions of PLGA-PCL phase separation and to measure the diameters and the number of islands of the PCL-rich regions (Meredith et al, 2003).

Atomic force microscopy (AFM). AFM measurements were performed using a TMX 1010 Stage Scanning Probe Microscope (ThermoMicroscopes, Sunnyvale, CA) operating in the air in contact mode (Meredith et al, 2003). The surface topography and Z-modulus of different locations on PLGA-PCL libraries was measured. The average surface roughness was calculated using arithmetic means of the deviation in height from the topology image mean values. The averaged height was determined from arithmetic means defined as the sum of all height values divided by the number of data points. Phase structures and harnesses were illustrated in Z-modulus pictures.

X-ray photoelectron spectroscopy (XPS). Composition and annealing temperature dependent surface compositions were analyzed by XPS (Surface Science SSX-100 with small spot ESCA spectrometer, Charles Evans & Associates, Sunnyvale, CA) with monochromatic Al K-alpha X-ray source (1486.6eV) (Klee et al, 2003). Survey scan spectrums were taken and surface elemental stoichiometries were determined from peak-area ratios (Niklason and Abbott et al, 2001).

Differential scanning calorimetry (DSC). Thermal analysis of the polymers was carried out with DSC (Seiko Instruments Inc., Chiba Japan) to calculate the effects of composition and annealing temperature on polymer crystallinity (van Dijkhuizen-

Radersma, 2003). Uniform homogenous samples (5-15 mg) were heated from -70 to 200°C at a rate of 10°C/min. Crystallinity was determined by the heat required for melting (mJ/mg).

Uniaxial mechanical analysis. Effects of ϕ_{PCL} on mechanical properties were assessed through uniaxial cyclic loading using a electromechanical testing system (DLL 650R, Eden Prairie, MN). Uniform individual films (200 μm thick) were stretched to 10% strain, allowed to recover for 2 min, and loaded again to 0.3N to failure. Linear (Young's) moduli, maximum stresses, yield strains, and recovery percentages (working strains) were determined from the stress-strain curves (Supplemental Figure 2).

Statistical analysis. Analytical results are expressed as means ± SEM. Comparison of multiple sample groups were performed using Tukey's protected t-tests in combination with analysis of variation (ANOVA). Comparisons of individual sample groups were performed using unpaired student t-test. For all statistics, $P<0.05$ was considered statistically significant.

5.4 Results

Characterization of phase-separated microstructures and physical properties. Crossed-polar optical microscope images [Figure 11(a)], reveal the diverse microstructures formed on T-ϕ gradient libraries as a result of PCL/PLGA phase separation and PCL crystallization (Meredith et al, 2003). The phase-separated microstructures had an amorphous PLGA-rich matrix containing dispersed semicrystalline PCL-rich regimes. Larger PCL regions with both semicontinuous and droplet morphologies were observed as ϕ_{PCL} increased, consistent with spinodal decomposition and nucleation-growth mechanisms of phase separation (Meredith and Aims, 2000). The diameter, *d*, of PCL-rich regimes increased with ϕ_{PCL} but showed a smaller dependence on *T* [Figure11(b)]. Either nucleation and growth rates of these PLGA-PCL phase-separated microstructures did not change much with *T*, or the annealing was stopped at a point where late-stage growth (Ostwald-ripening) had "equalized" the microstructure sizes at various *T* values. The diameters covered the ranges: $21.8 < d < 31.8$ μm (high ϕ_{PCL}), $11.4 < d < 17.6$ μm (mid ϕ_{PCL}) and $5.4 < d < 7.7$ μm (low ϕ_{PCL}).

The average surface roughness [Figure 11(c)] was highest at the mid ϕ_{PCL} –mid *T* regime and the second highest at the high ϕ_{PCL} –mid *T* regime. The other regimes did not show significant roughness differences among them. 3D lateral force AFM images revealed clear height differences between amorphous PLGA (blue) and peaked semicrystalline PCL (white) [Figure 11(d)]. It shows that the highest height difference was at the mid ϕ_{PCL} –mid *T* regime, with a negative value at the high ϕ_{PCL} –mid *T* regime. Mid ϕ_{PCL} –mid *T* regions possessed more overall concaved geometry surface structures than the other regimes, which showed predominantly convex island structures.

AFM Z-modulus analysis showed that the transition, or boundary, regions between PCL and PLGA exhibited intermediate hardness values between that of the hard crystallized PCL islands and softer PLGA matrix [Figure 14(b)]. DSC was used to investigate the thermal properties and crystallinity of each regime (Pyne et al, 2003; van Dijkhuizen-Radersma, 2003) [Figure 14(c)]. Individual uniform films were prepared at each of the high, medium, and low annealing *T*, ϕ_{PCL} conditions observed on the libraries. As expected, the overall crystallinity followed the PCL composition. The crystallinity at high ϕ_{PCL} = 0.375 showed no significant dependence on the annealing temperature. At middle ϕ_{PCL} = 0.225, crystallinity *decreased* significantly as annealing T was raised to 85 ^{o}C and again at 110 ^{o}C ($P<0.001$), compared to 50 ^{o}C. However, at low ϕ_{PCL} = 0.076 the crystallinity *increased* significantly as annealing T was raised from 50 ^{o}C to 85 ^{o}C and 110 ^{o}C, which was opposite of the pattern observed at mid ϕ_{PCL}. It is clear from comparison of the AFM and DSC characterization that the relative area of hard domains (as qualitatively indicated by AFM) followed the overall crystallinity. The mid ϕ_{PCL} – high T regimes showed: (1) decreased crystallinity and hardness relative to mid- and low-T regions at mid ϕ_{PCL}, and (2) intermediate crystallinity and hardness relative to all other ϕ_{PCL} –high T regimes.

SMC adhesion, population distribution, and viability. SMC cultured directly on the libraries (postannealing) for 8 h showed the highest adhesion at mid ϕ_{PCL} –mid T conditions (adhesion > 15%, $P < 0.05$) relative to other chip regions (adhesion 8 to 10 %), which showed no significant differences among them [Figure 12(a)]. Adhesion in each T, ϕ_{PCL} region is represented as a percentage of total cells on the entire library. SMC adhesion was strongly correlated with the average surface roughness and the direct height difference between crystallized PCL and amorphous PLGA structures.

SMC showed a significant area-dependent cell population increase in the mid-to-high ϕ_{PCL} and high T regions at day 7 in comparison with day 1 [Figure 12(b)]. This trend is apparent in both fluorescence microscopy of individual chip regions and whole-library phosophoimaging scans, indicated that specific polymeric properties in those regimes strongly influenced SMC interactions with the scaffolds (Zhang et al, 2004; Cheng Z and Teoh, 2004; Niklason and Abbott, 2001; Niklason and Gao, 1999; Prabhakar et al, 2003).

The quantified 7 day cultured SMC population was largest at the mid ϕ_{PCL} –high T regime and second largest at high ϕ_{PCL} –high T [Figure 13(a)]. The other regimes didn't show any significant differences among them.

SMC viability (propidium iodide) at days 1 and 7 showed a statistically significant ($P < 0.05$) increase with increasing ϕ_{PCL} (Supplemental Figure 1), for example from 70 % to 90 % at day 1. Like the PCL diameter, this trend depended very little on T and overall SMC viability was increased at 7 day compared with 1 day. Even without the T effect, the mechanical properties showed apparent changes with increasing ϕ_{PCL} in blending (Supplemental Figure 2).

SMC proliferation. At 1 day, mid ϕ_{PCL} –high T and high ϕ_{PCL} –high T regimes also showed the highest percentages of proliferating SMC [Figure 13(b)]. The other regimes didn't show any significant differences in the proliferation. The 7-day proliferation data [Figure 13(c)] exhibited an increase in most regimes compared to day 1. There was no significant difference in day 7 proliferation among the regimes with the exception of the low ϕ_{PCL} – low T regime, which showed significantly fewer proliferating SMCs. A strong linkage between 7 day population [Figure 13(a)] and 1 day proliferation [Figure 13(b)] was observed; however, the higher cell populations at mid ϕ_{PCL} – high T regimes than at high ϕ_{PCL} – high T regimes could not be explained by SMC proliferation alone. This observation suggests that other effects are involved in the population dependence on surface features.

SMC aggregation related with surface hardness, and thermal analysis for crystallinity. Shortly after cell seeding, SMCs were observed to aggregate prevalently in the boundary regions between crystallized PCL islands (white) and the PLGA matrix (dark) [Figure 14(a)]. As the regime-dependent change of crystallinity showed [Figure 14(c)], it appears that the high SMC population at the mid ϕ_{PCL} –high T regime correlates with crystalline surface hardness (Washburn et al 2004), supported by micrometer scale surface hardness characterization from Figures 14(a), (b). Based upon the AFM [Figure 14(b)] and DSC [Figure 14(c)] data, this behavior suggests a correlation between the local aggregation of SMCs and the polymer surface hardness, crystallinity, and feature height.

Surface-composition-dependent serum protein adsorption and SMC protein production. Localized serum protein (from culture medium) accumulation was visualized using ^{35}S- methionine at 3 days without SMC seeding [Figure 15(a)]. The dark regions, indicating protein accumulation in the phospho-scan images, predominantly occupied the mid ϕ_{PCL} = 0.225 to high ϕ_{PCL} = 0.375 regimes at all T. This accumulation extended slightly into the low ϕ_{PCL} = 0.15 – high T regime as well. XPS surface composition analysis indicated that the polymer blend surfaces were comprised mainly of oxygen, carbon, and hydrogen [Figure 15(b)]. There were no surface composition changes following shifts in the annealing temperature. However, averaged carbon contents increased from 52.5 % at low ϕ_{PCL} = 0.076 to 70.5 % at mid ϕ_{PCL} = 0.225, and relative oxygen contents decreased. Interestingly, there were no remarkable changes from ϕ_{PCL} = 0.225 to ϕ_{PCL} = 0.375. These trends in the average surface % carbon content must be due to selective expression of certain molecular segments over others at the surface, since the bulk % carbon in the PCL and PLGA monomers are both 1/3. Hence, the bulk % carbon does not change with composition. It is likely that methylene groups are predominant on the surface due to their lower surface energy contribution compared to the ether and carbonyl moieties. So, differences in % surface carbon probably derive from the different fractions of PCL-rich versus PLGA-rich surface domains. PCL-rich domains have more methylene groups that can be expressed on the surface, which would be in line with the XPS data. Comparing the qualitative description of protein deposition with quantitative surface compositions indicates that serum protein accumulation coincides the increased hydrophobicity on the carbon rich surface regions of the library. Following SMC seeding, protein expression maps displayed different patterns [Figure 15(c)]. Compared to the pattern of the serum protein accumulation, 1-day protein production showed aggregation in distinct spots predominantly at mid and high ϕ_{PCL} – high T regimes. This SMC protein production matched the patterns observed in 1-day SMC proliferation [Figure 13(b)]. By 3 days, the protein production maps expanded to include high ϕ_{PCL} - mid T and low T regimes. The 7-day protein production maps eventually covered the entire library surface except for the low ϕ_{PCL} – low T regime. These patterns also correlated with the 7-day SMC proliferation [Figure 13(c)]. These results imply that SMC proliferation was likely based on protein production mediated interaction, more so than the serum-protein accumulation.

Verification of combinatorial library SMC adhesion and proliferation data. Individual uniform films were investigated to verify SMC adhesion and proliferation findings. Figure 16(a) shows SMC adhesion was highest in $\phi_{PCL} = 0.225$, $T = 85$ ^{o}C samples. These conditions corresponded to the mid ϕ_{PCL} – mid T regions of the combinatorial chips and matched the previous findings [Figure 12(a)]. Cell proliferation data [Figure 16(b)] also matched the combinatorial chip data [Figure 13(b), (c)]. The ϕ_{PCL} = 0.225, $T = 110$ ^{o}C samples showed significantly higher SMC proliferation than the other samples at 1 day. The uniform samples at other T, ϕ_{PCL} didn't show any significant difference among them. At 7 days, the $\phi_{PCL} = 0.225$, $T = 110$ °C and $\phi_{PCL} = 0.225$, $T = 85$ °C samples and cover glass control showed a significant increase of SMC proliferation compared to their 1 day counterparts. Specifically, the $\phi_{PCL} = 0.225$, $T = 85$ °C samples showed the most significant increases ($P<0.001$) at 7 days, which matched the combinatorial chip data. At 7 days, the $\phi_{PCL} = 0.225$, $T = 110$ °C and $\phi_{PCL} = 0.225$, $T = 85$ °C samples showed significantly higher cell proliferation rates than the other individual samples. However, the $\phi_{PCL} = 0.375$, $T = 110$ °C samples that represented the edge of the highest ϕ_{PCL} – high T in the combinatorial chip did not show any improvement of SMC proliferation. All the individual film experiments verified the combinatorial chip findings and correlations among SMC adhesion and proliferation to the polymeric properties.

5.5 Figures and Legends

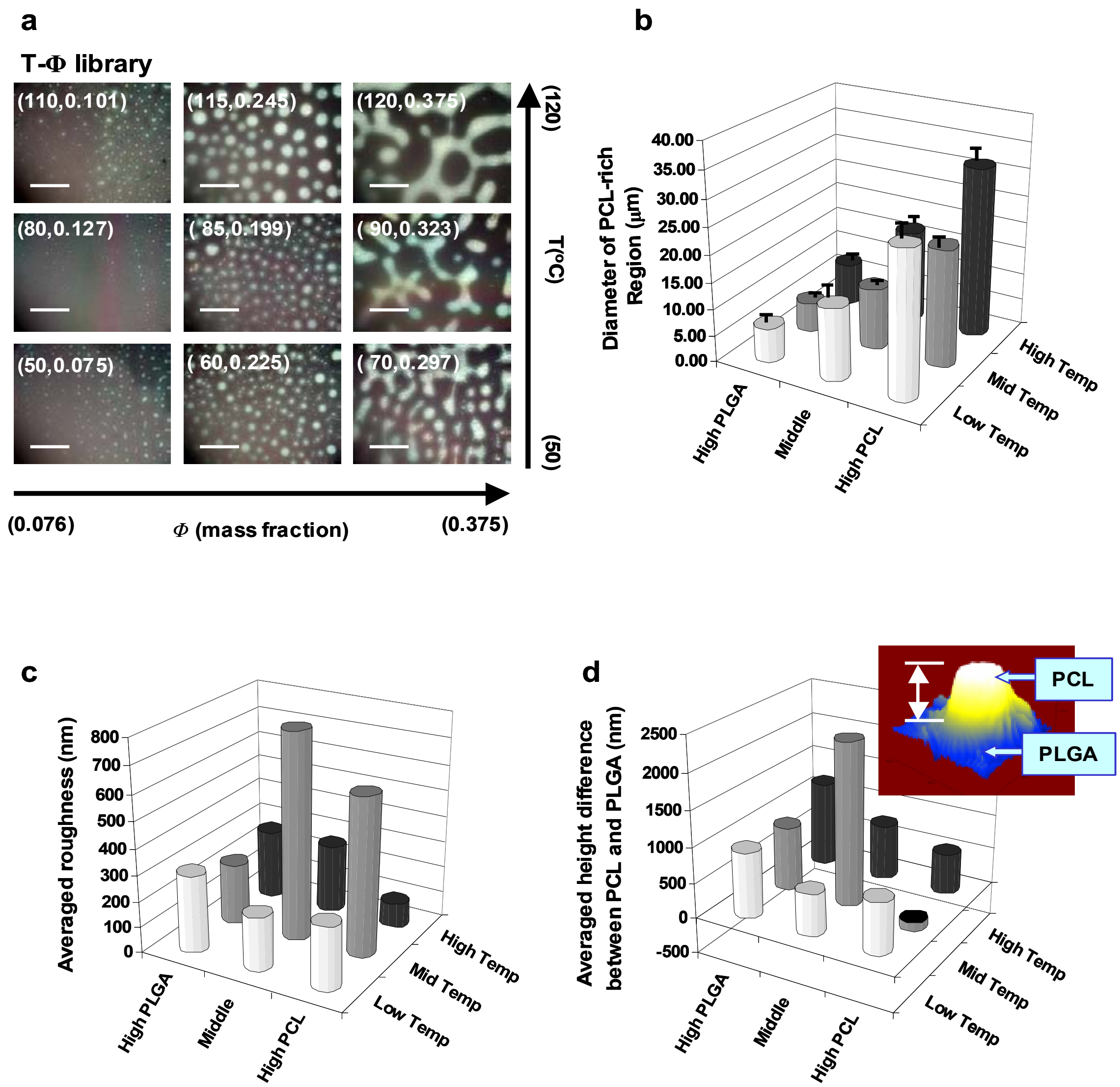

Figure 11. Characterization of phase-separated microstructures and surface roughness. (a) Crossed-polar optical micrographs of selected regions from a PLGA/PCL T- ϕ_{PCL} library illustrate the diverse morphologies generated through the phase separation and crystallization. White areas are crystalline PCL; dark areas are amorphous PLGA possibly containing some PCL. The scale bar is 60 μm and the numbers in parentheses are (T, ϕ_{PCL}). (b) The diameter of PCL-rich regimes was measured using crossed-polar optical microscopy. Means were obtained from 4 different spots at each regime for 3 independent library chips. (c) Average surface roughness was obtained from arithmetic means of the deviation in height from the AFM topology image mean values. (d) Images (upper) from three-dimensional AFM lateral force represent the clear height difference

between two polymer domains. Averaged heights of both the polymer domains were calculated as arithmetic means from the sums of all height values divided by the number of data points.

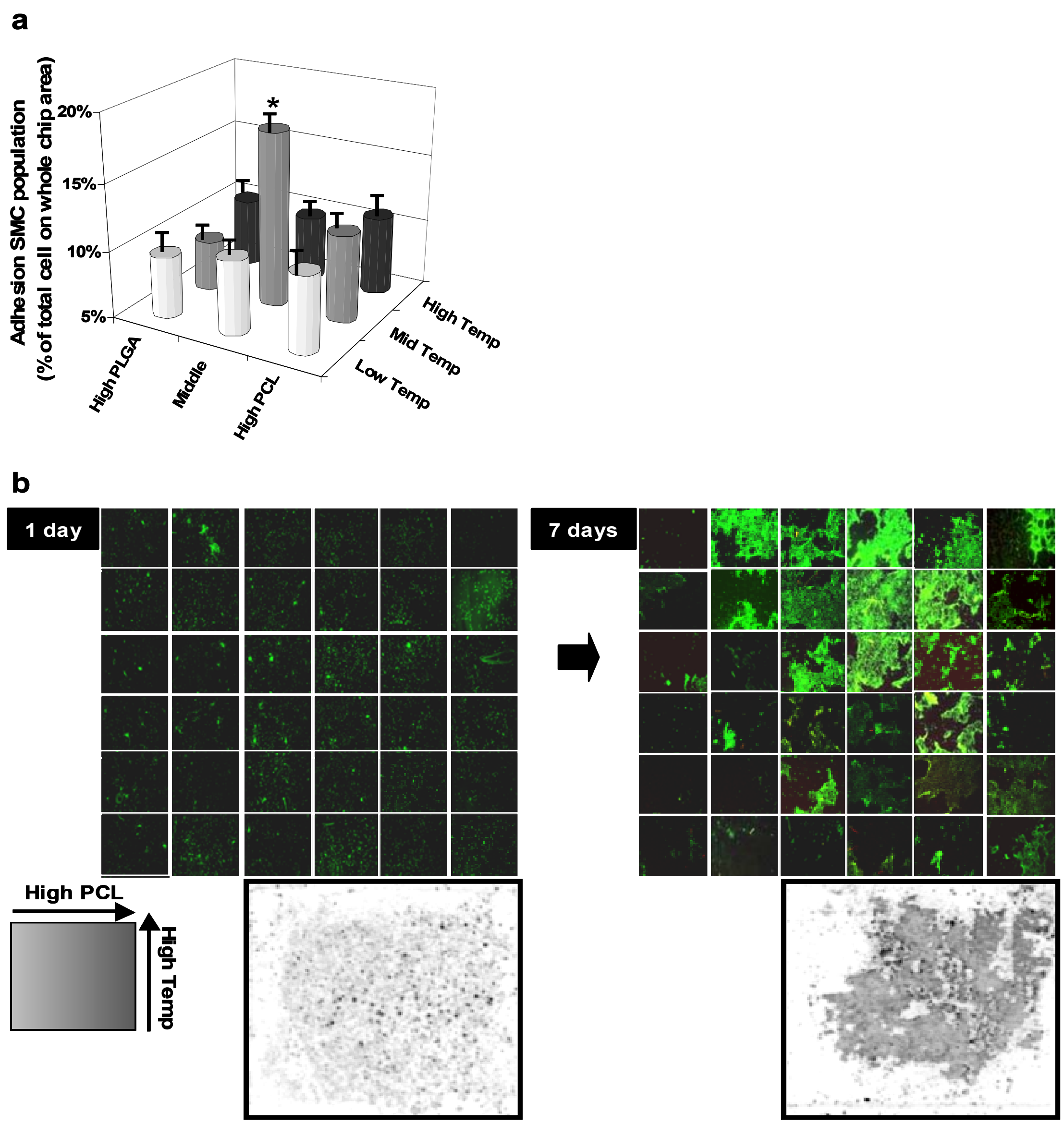

Figure 12. SMC adhesion and population distribution. (a) Adhered cell population was represented as a percentage of total SMC population on the whole chip. Means were obtained from 4 different spots at each 9 regime for 3 independent chip experiments. (*) $P < 0.05$. (b) SMC cultured directly on the libraries (postannealing) were visualized at 1 and 7 days with SYBR™ green nucleus staining in fluorescent micrographs and as black dots in the whole chip area scan images. Representative fluorescence and phospho scan images from three independent experiments are illustrated.

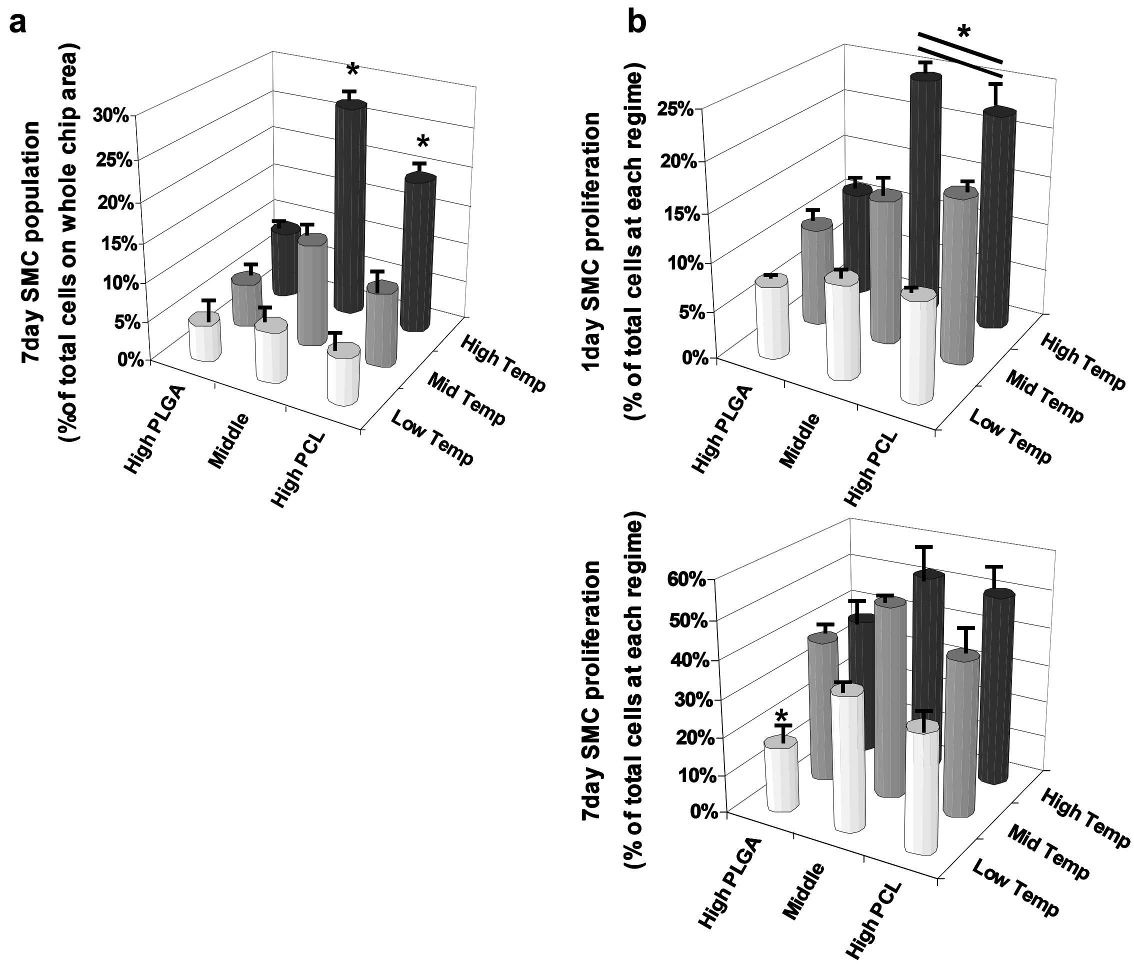

Figure 13. Area-dependent SMC populations are linked to proliferation rates. (a) Each regime SMC population at 7 days is represented as a percentage of total SMC population on the whole chip. SMC proliferation rates were calculated as a percentage of BrdU positive cells at 1day (b) and 7 days (c). Means were obtained using 4 random spots in each of the 9 regions of 3 independent chip experiments. (*) P < 0.05.

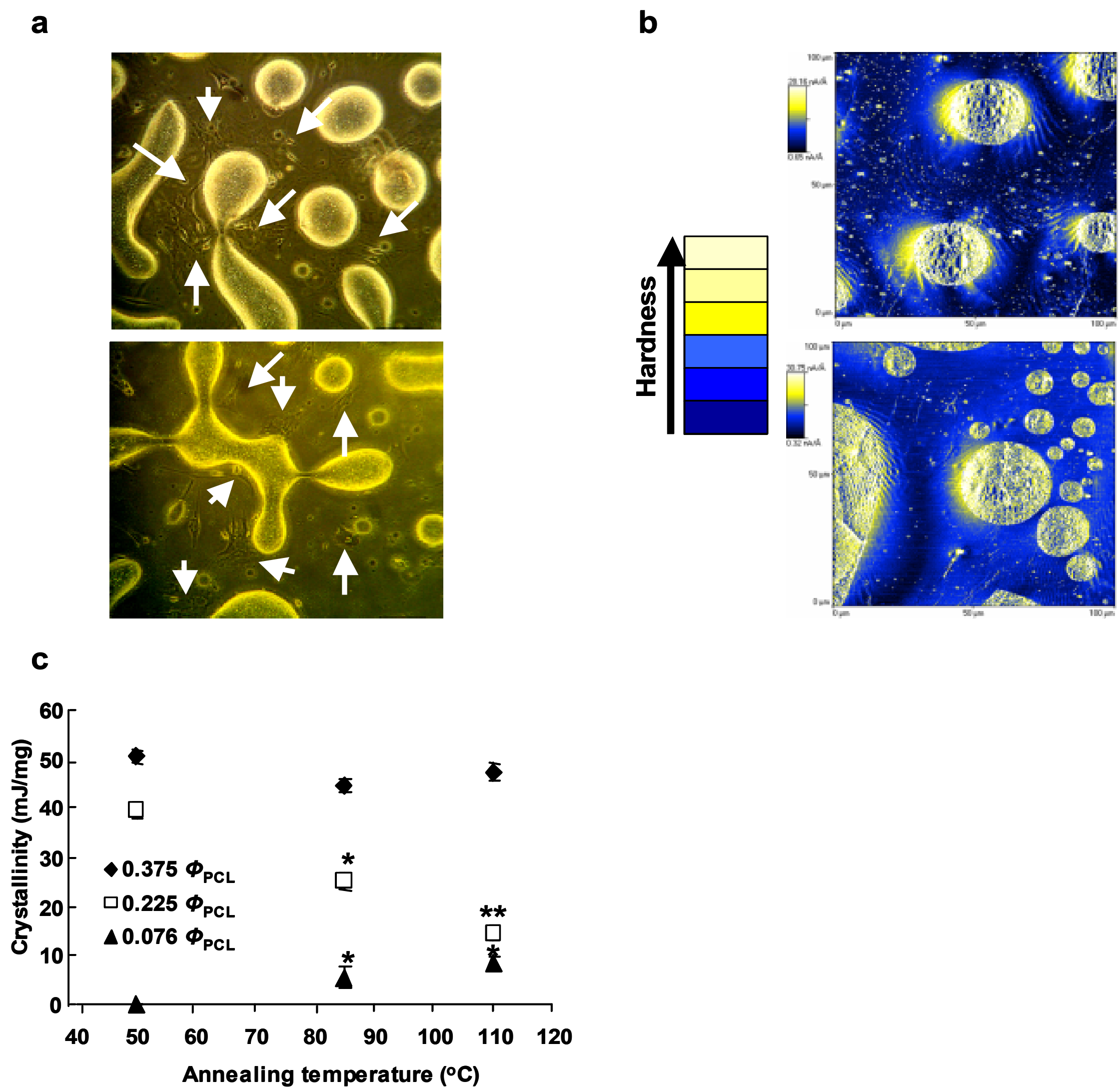

Figure 14. SMC aggregation correlated with surface hardness and crystallinity. (a) Arrows show SMC aggregation around the boundary regions between the two polymer phases (10 × 10 grid of images). (b) AFM Z-modulus images represent surface hardness (100 X 100 μm size of images). Color changes from dark blue to light yellow represent increases in hardness. (c) Crystallinity was measured by DSC thermal analysis. Means were obtained from 3 independent experiments. (*) $P < 0.05$, (**) $P<0.001$ vs. at 50 °C annealing temperature.

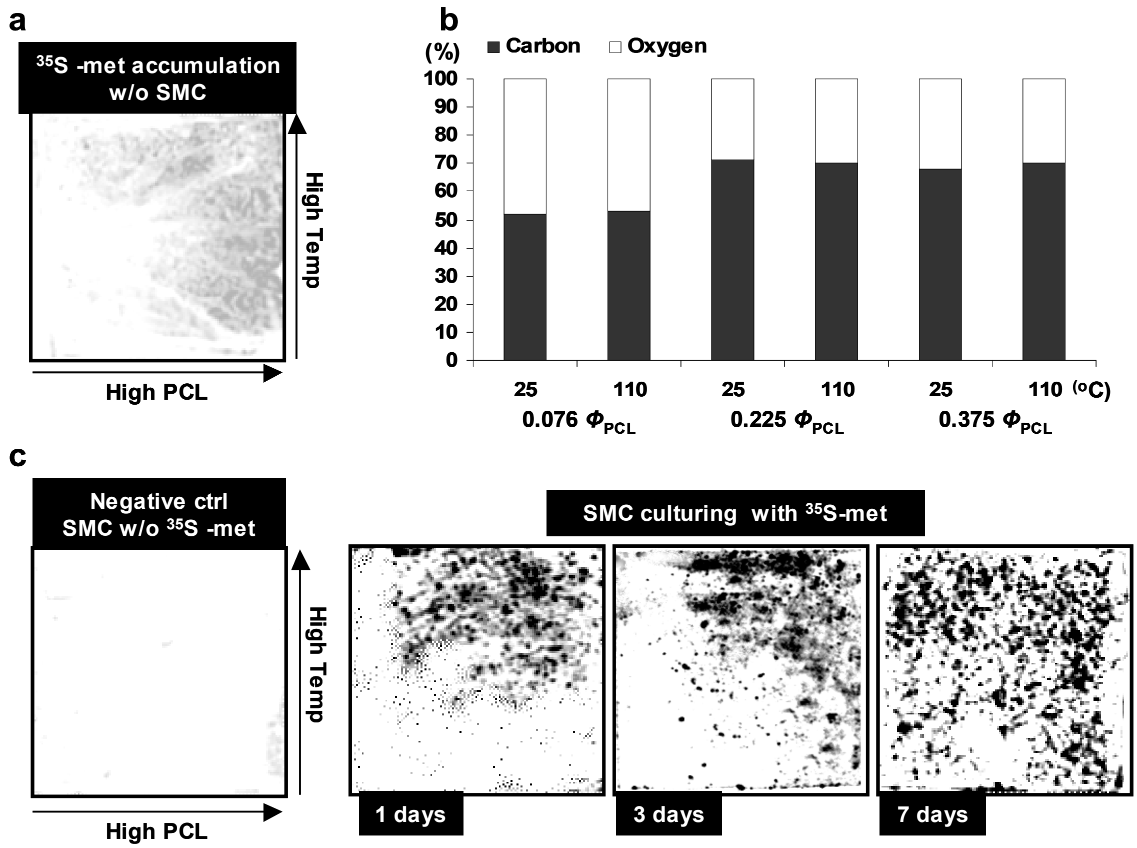

Figure 15. Surface composition dependent protein accumulation from culture medium and SMC protein production. (a) The dark areas indicate the culture medium protein accumulation dominant area without SMC seeding at 3 days in phospho scan image of the whole chip. (b) Surface compositions were analyzed by XPS using individual uniform chips. Surface elemental stoichiometries were determined from peak-area ratios of survey scan spectrum. (c) Black dots indicate SMC protein productions as through ^{35}S-methionine phospho scan images. 1day images for SMC cultured without ^{35}S- methionine were taken as negative controls. Representative phospho scan images of three independent experiments are shown.

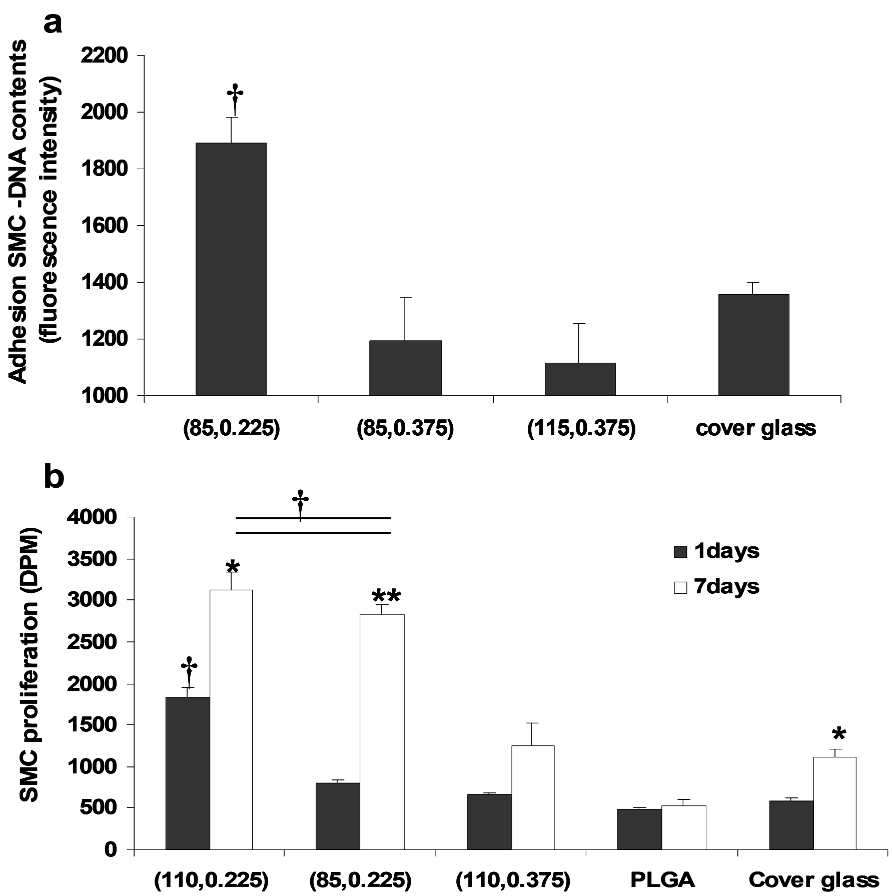

Figure 16. Verification of combinatorial libraries SMC adhesion and proliferation using individual uniform films. The numbers in parentheses show (T, ϕ_{PCL}). The processing conditions (T, ϕ_{PCL}) were selected based on the combinatorial chip results. Glass coverslips were used as controls. (a) Fluorescence intensities of DNA labeled with SYBR™ green were measured to analyze SMC adhesion at 8 hours post seeding. (b) SMC proliferation was measured using ^{3}H-thymidine incorporation at 1 and 7 days. Means were obtained from 3 independent experiments. **(†)** $P<0.05$ the adhesion or proliferation on the sample at the same evaluation time point or day vs. the other samples and (*) $P < 0.05$, (**) $P<0.001$ proliferation at 7day vs.1day.

Supplemental Table 1.

	PLGA (Poly lactic–co –glycolic acid)	PCL (Poly ε–caprolactone)
Structure	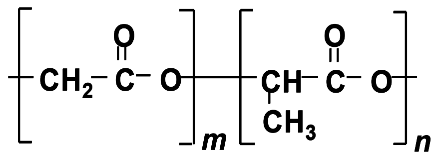	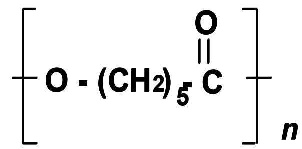
Mw	2-5X10^5	1-2X10^6
Degradation	1- 4 months	Over 1 year
Crystallinity	Amorphous	Semi-crystalline
Tg / Tm (°C)	55 / 200	- 60 / 60
Tensile Modulus (GPa)	8.6	0.15

Comparison of the properties between PLGA and PCL used in this study.

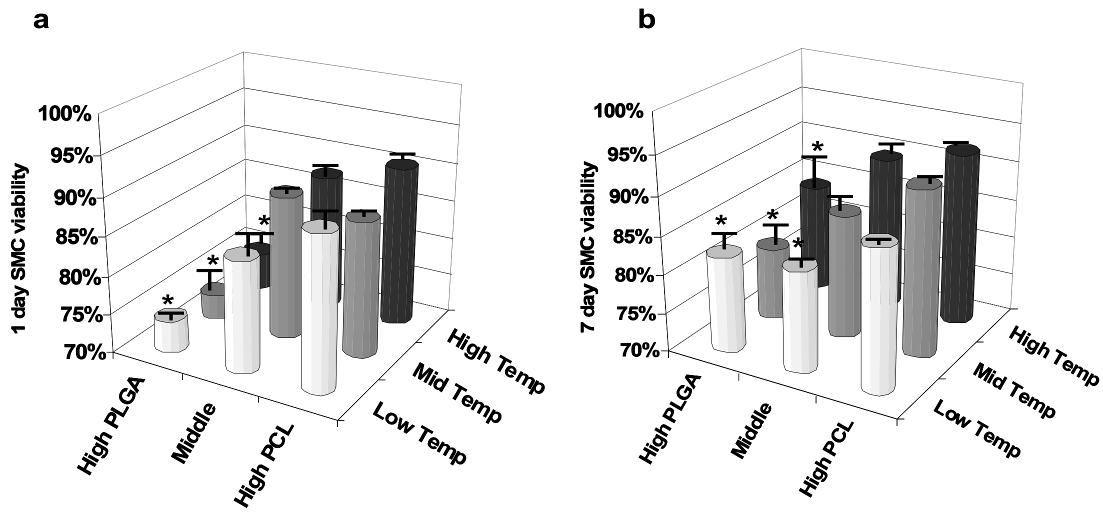

Supplemental Figure 1. SMC viability decreased at high PLGA compositions. (a) 1 day and (b) 7 day viability was measured by counting the percentage of cells that took up propidium iodide (PI) in each regime. Means were obtained from 4 spots at each regime in 3 independent chip experiments. (*) $P < 0.05$ vs. the high ϕ_{PCL} at the corresponding temperature.

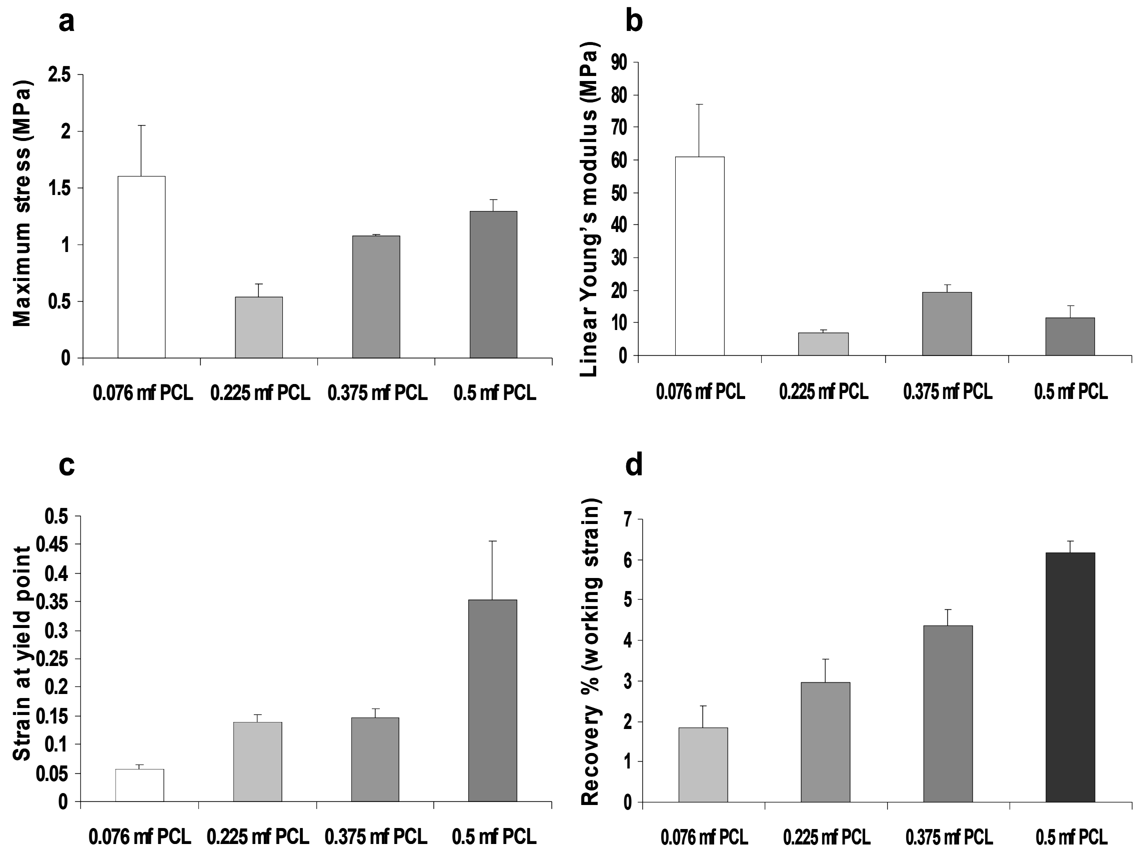

Supplemental Figure 2. Mechanical properties of blended PLGA/PCL were dependent on Φ_{PCL} . (a) Maximum stress, (b) Linear (Young's) modulus, (c) Strain at yield point and (d) Recovery percentage (working strain) were determined from stress-strain curves of uniformly fabricated polymer films; mass fraction (mf). (n=3)

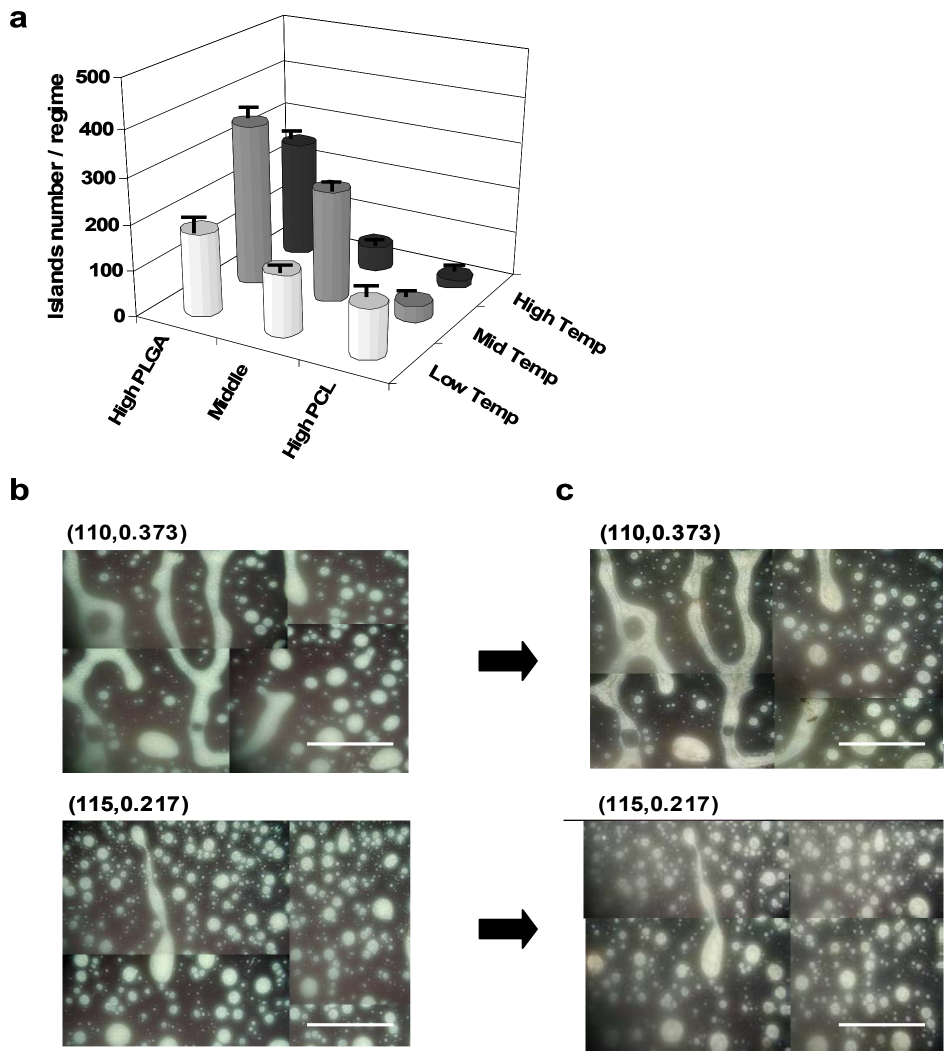

Supplemental Figure 3. Crossed-polar optical microscopy reveals changes in crystalline microstructure following SMC culture. (a) Number of PCL-rich islands. Means were obtained from 4 different spots at each regime for 3 independent chip experiments. Chip surfaces were compared (b) before cell seeding and (c) after 14 days of SMC culture. Scale bar represents 60 μm and the numbers in parentheses are (T (^{o}C), ϕ_{PCL}).

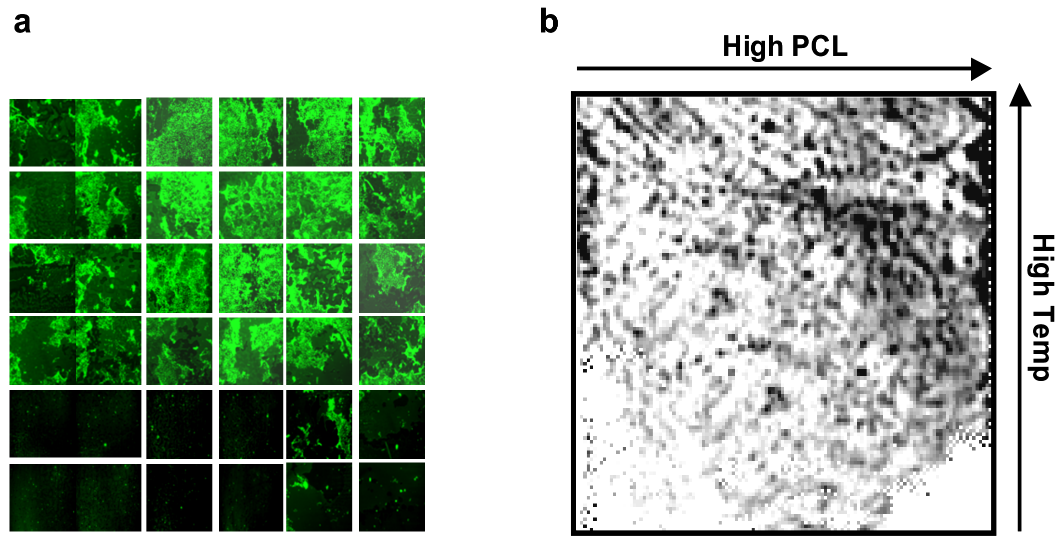

Supplemental Figure 4. After 14 days of culture, SMC populations on the combinatorial chip coincided with areas of high protein production. (a) Area-dependent SMC populations were visualized at 14 days using SYBR green nuclei labeling and reconstructed using representative fluorescence images. (b) Phospho-scan images of entire chips show regions of ^{35}S-methionine labeled protein production (black dots) after 14 days of SMC culture. Arrows indicate the orientation of T and ϕ_{PCL} gradients.

5.6 Discussion

The combinatorial polymer libraries provided a high-throughput technique to investigate the effects of varying polymer properties on SMC interactions in a rapid, efficient, and accurate manner. In particular, the method provided rapid identification of blended polymeric properties that promote (or reduce) cell adhesion and proliferation for discovery of a truly "bioactive" scaffold. Moreover, the high-throughput libraries identify quickly the major trends, so that more careful and detailed experiments can be performed afterwards to investigate fundamental mechanisms underlying the behavior. In this way, the most expensive and time-consuming assays can be focused onto the regions of composition and surface structure that are already known to yield the most information. In this manner, the combinatorial assay technique couples nicely with traditional cell culture techniques.

Previous studies have indicated the strong influence of surface roughness on cell interactions (Bagno A et al, 2004; Thapa et al, 2004; Miller et al, 2004), observed also in this study in terms of the direct height difference between crystallized and amorphous structures, and the averaged surface roughness [Figure 12].

A strong correlation between SMC population and proliferation was shown in this study. However, the higher cell populations were observed at mid ϕ_{PCL} –high T regimes at 7 days, even though the mid- and high-PCL – high T regimes showed no significant differences in proliferation rate [Figure 13]. From the DSC thermal analysis [Figure 14(c)], the decreased crystallinity in mid ϕ_{PCL} –high T regime was observed compared to the same or higher ϕ_{PCL}. Supplemental Figure 3(a) shows the area-dependent change in the number of crystalline islands and especially small number at mid ϕ_{PCL} –high T

regimes compared to the same ϕ_{PCL}, regimes, which also likely implied the effects of high T on crystallinity in mid ϕ_{PCL}. This suggested that the SMC aggregation might be caused by the surface hardness changes relating with crystallinity like osteoblast (Zhang et al, 2004; ter Brugge et al, 2003; Yang et al, 2003). The strong possibilities between SMC aggregation and the surface hardness were shown in the micro scale investigation during initial culture periods [Figure 14(a),(b)], which could support furthermore the macro-scale SMC aggregation across the each regime.

An analysis of protein accumulation and surface composition showed that protein accumulation from the culture medium occurred predominantly at the hydrophobic carbon-rich surface regions (Collier et al 1997) [Figure 15(a), (b)]. This indicated the additional importance of the surface properties on biological interactions with scaffolds. Annealing temperatures did not affect protein accumulation from the culture medium, however, culturing SMC showed temperature dependent differences on SMC protein production [Figure 15(c)]. The importance of serum protein including fibronectin absorption on the cell adhesion on the matrix has been previously described (El-Ghannam et al, 1999), however, our study provided another possibility that the initial SMC interaction can be affected by the direct cell contact with the surface properties of the polymer scaffolds (Gugala and Gogolewski, 2004; Itala et al 2002), because the high SMC adhesion and 1-day high cell proliferation regimes were different from the high culture medium protein accumulation regimes. Supplemental Figure 3(b),(c) showed, even after 14 days culturing, there was no significant change in overall surface crystalline micro-structure, but 14-day localized cell populations were different from their 1- and 7-day counterparts [Figure 11(c)], which indicated the direct cell contact with the surface properties is not enough to explain long-term SMC interaction. Since strong correlations were observed between the high SMC proliferation regimes and the high SMC protein production regimes, it can be strongly suggested that even if the initial culture period SMC interactions can be affected by the direct cell contact with the surface properties, SMC proliferations are likely stimulated more through SMC protein production-mediated interactions. Supplemental Figure 4 supports this suggestion furthermore by showing the matched patterns between 14-day localized SMC population and protein production map.

Literature evidence also shows that polymer surface chemistry, microstructure, and roughness influence cell adhesion, proliferation, and differentiation (Meredith et al, 2003; Zhang et al, 2004; Cheng and Teoh, 2004; Niklason and Abbott et al, 2001; Bagno et al, 2004; Yang et la, 2003; Huang and Ingber, 2000; Wieland et al 2002). Future experiments, however, will be required to elucidate the potential issues regarding the effects of polymer properties, protein accumulation, and production (Collier et al, 1997; El-Ghannam et al, 1999; Gugala and Gogolewski, 2004; Itala et al, 2002; Boyan et al, 1998; García et al, 1999) on SMC proliferation, migration, and adhesion relating with intracellular signaling.

The individual film experiments verified the combinatorial chip findings that correlated SMC adhesion and proliferation to the polymeric properties. All these studies revealed a previously unknown processing temperature and blending compositions for two well-known polymers, which optimized SMC interactions.

CHAPTER 6

Overall Conclusion

This study showed that 3D biodegradable scaffolds can be developed using a new method to control the thickness and pore size employing a knife-edge coater with a computer-controlled motion stage and phase-transitional salts. The comparative study of fast vs. slow degrading 3D scaffolds indicated that fast degradation negatively affects cell viability and migration into the scaffold *in vitro* and *in vivo*. This effect is likely due to the significant acidification of the local environment due to the polymer degradation. It is also reported that the angiogenic response developed within the scaffolds implanted *in vivo* was related to the presence of an inflammatory response. These results should contribute to a better understanding of the cell-biodegradable scaffold interactions necessary to optimize the manufacturing and survival of tissue constructs.

The study of the function of MMP-9 on cell-matrix interactions for function and survival of vascular constructs showed MMP-9 deficiency did not affect collagen mRNA production or biodegradable polymer scaffold degradation, but net collagen accumulation was greater in cultures of MMP-9 KO than in WT SMC, because of degradation by MMP-9. Ascorbic acid treatment enhanced collagen deposition by MMP-9 KO compared to WT SMC at 3 days, but at 7 days this effect was reversed. MMP-9 improved fibrillogenesis of collagen, significantly more upon ascorbic acid treatment. This study showed that MMP-9 deficiency led to a dramatic decrease in inflammatory cell invasion and capillary formation within biodegradable polymer scaffolds *in vivo*. Importantly, these results support the role of MMP-9 in eliciting an appropriate host inflammatory response in order to enhance the local recruitment of vasculature to tissue engineered constructs, essential for their integration as well as their long-term survival and function. Overall, it could be concluded that inhibition of MMP-9 may negatively affect remodeling of collagen on scaffolds and decrease survival of implants by decreasing angiogenesis.

Temperature-composition combinatorial polymer libraries were utilized to investigate the effect of surfaces of blended PLGA and PCL on MASMC to optimize polymer compositions and processing conditions for “bioactive” scaffold. These libraries tested the diverse distinguishable surface properties possible in a single experiment, such as phase-separated microstructures, roughness, hardness, and crystallinity. SMC adhesion was strongly correlated with the average surface roughness and the direct height difference between crystallized PCL and amorphous PLGA structures. SMC behavior on the libraries suggests a correlation between the local aggregation of SMCs and the polymer surface hardness, crystallinity, and feature height. SMC proliferation was likely based on protein production mediated interaction, more so than the serum-protein accumulation. The individual film experiments verified the combinatorial chip findings that correlated SMC adhesion and proliferation to the polymeric properties. All these studies revealed a previously unknown processing temperature and blending compositions for two well-known polymers, which optimized SMC interactions.

MMP-9 was crucial for the remodeling process and angiogenesis required for the function and survival of the tissue substrates. These studies showed the importance of understanding effects of scaffold degradation rate on 3D cell growth and angiogenesis.

The novel combinatorial polymer blending method was suggested for applying “bioactive scaffold by determining the ideal biodegradable polymer processing conditions.

CHAPTER 7

Future Studies

Further investigations about the negative effect of lowering local pH caused by fast degradation, is necessary to verify the effect of different serum protein deposition between hydrophobic (PCL) and hydrophilic (PLGA) surfaces. These could be performed by controlling the buffering effect of culture medium, then investigating the serum protein deposition effect on series *in vitro* and *in vivo* cellular viability or functional assay.

In treatment of ascorbic acid, collagen type 1 mRNA expression was affected by MMP-9 deficiency. Ascorbic acid is a well-known reactive oxygen species scavenger, so various future studies are possible to investigate the potential relationship between oxidative stress and MMP-9 from the view point of physiological or intracellular signaling pathways.

Further detailed experiments will be required to elucidate the potential correlations regarding the effects of polymer properties of combinatorial libraries on the SMC adhesion, aggregation, and proliferation. Also the further more experiments will be required to compare SMC interaction between the founded surface properties and tissue culture plates (TCPS). Interesting future studies that can be investigated specifically, are the effects of protein accumulation and production on SMC proliferation, migration, and adhesion relating with intracellular signaling. In addition, the mechanical properties of the blended polymers vary as a function of ϕ_{PCL}. However, potential further experiments are required to investigate the effect of annealing temperature and following surface structure change on the mechanical strength.

These studies may provide solutions for sourcing autologous tissue by applying this newly investigated cell scaffold interaction property to drive differentiation of stem cells to vascular cells, as well as developing 3D tissue engineered vascular constructs that can synchronize degradation time with remodeling of natural vascular tissue. Specifically in process of developing 3D tubular form of scaffolds, further detail considerations are necessary to maximize the benefit of blended polymer construct based on combinatorial chip findings.

REFERENCES

Acar C, Jebara VA, Portoghese M, Beyssen B, Pagny JY, Grare P, Chachques JC, Fabiani JN, Deloche A, Guermonprez JL. Revival of the radial artery for coronary artery bypass grafting. Ann Thorac Surg. 1992;54:652-9; discussion 659-60.

Agrawal CH, D. Schmitz, JP. Athanasiou, KA. Elevated temperature degradation of a 50:50 of PLA-PGA. Tissue Eng. 1998;3:345-52.

Agrawal CM, McKinney JS, Lanctot D, Athanasiou KA. Effects of fluid flow on the in vitro degradation kinetics of biodegradable scaffolds for tissue engineering. Biomaterials. 2000;21:2443-52.

Athanasiou K, Schmitz. JP, Agrawal. CM. The effect of porosity on degradation of PLA-PGA implants. Tissue Eng. 1998;4:53-63.

Bader A, Steinhoff G, Strobl K, Schilling T, Brandes G, Mertsching H, Tsikas D, Froelich J, Haverich A. Engineering of human vascular aortic tissue based on a xenogeneic starter matrix. Transplantation. 2000;70:7-14.

Bagno A, Genovese M, Luchini A, Dettin M, Conconi MT, Menti AM, Parnigotto PP, Di Bello C. Contact profilometry and correspondence analysis to correlate surface properties and cell adhesion in vitro of uncoated and coated Ti and Ti6Al4V disks. Biomaterials. 2004;25:2437-45.

Baker AH, Zaltsman AB, George SJ, Newby AC. Divergent effects of tissue inhibitor of metalloproteinase-1, -2, or -3 overexpression on rat vascular smooth muscle cell invasion, proliferation, and death in vitro. TIMP-3 promotes apoptosis. J Clin Invest. 1998;101:1478-87.

Bendeck MP, Irvin C, Reidy M, Smith L, Mulholland D, Horton M, Giachelli CM. Smooth muscle cell matrix metalloproteinase production is stimulated via alpha(v)beta(3) integrin. Arterioscler Thromb Vasc Biol. 2000;20:1467-72.

Bergsma TM, Grandjean JG, Voors AA, Boonstra PW, den Heyer P, Ebels T. Low recurrence of angina pectoris after coronary artery bypass graft surgery with bilateral internal thoracic and right gastroepiploic arteries. Circulation. 1998;97:2402-5.

Boyan BD, Batzer R, Kieswetter K, Liu Y, Cochran DL, Szmuckler-Moncler S, Dean DD, Schwartz Z. Titanium surface roughness alters responsiveness of MG63 osteoblast-like cells to 1 alpha,25-(OH)2D3. J Biomed Mater Res. 1998;39:77-85.

Brocchini S, James K, Tangpasuthadol V, Kohn J. Structure-property correlations in a combinatorial library of degradable biomaterials. J Biomed Mater Res. 1998;42:66-75.

Campbell JH, Efendy JL, Campbell GR. Novel vascular graft grown within recipient's own peritoneal cavity. Circ Res. 1999;85:1173-8.

Can ZE, AR. Apaydin. Demirseren, E. Sabuncuoglu, B. Yormuk, E. Tissue engineering of high density porous polyethylene implant for three-dimensional reconstruction: an experimental study. Scand J Plastic Reconst Surg & Hand Surg. 2000;34:9-14.

Canver CC. Conduit options in coronary artery bypass surgery. Chest. 1995;108:1150-5.

Cheng Z, Teoh SH. Surface modification of ultra thin poly (epsilon-caprolactone) films using acrylic acid and collagen. Biomaterials. 2004;25:1991-2001.

Chicurel M. Faster, better, cheaper genotyping. Nature. 2001;412:580-2.

Cho A, Reidy MA. Matrix metalloproteinase-9 is necessary for the regulation of smooth muscle cell replication and migration after arterial injury. Circ Res. 2002;91:845-51.

Chu CF, Lu A, Liszkowski M, Sipehia R. Enhanced growth of animal and human endothelial cells on biodegradable polymers. Biochim Biophys Acta. 1999;1472:479-85.

Collier TO, Jenney CR, DeFife KM, Anderson JM. Protein adsorption on chemically modified surfaces. Biomed Sci Instrum. 1997;33:178-83.

Cooley DA. Coronary bypass grafting with bilateral internal thoracic arteries and the right gastroepiploic artery. Circulation. 1998;97:2384-5.

Corden TJ, Jones IA, Rudd CD, Christian P, Downes S, McDougall KE. Physical and biocompatibility properties of poly-epsilon-caprolactone produced using in situ polymerisation: a novel manufacturing technique for long-fibre composite materials. Biomaterials. 2000;21:713-24.

Cowan KN, Jones PL, Rabinovitch M. Elastase and matrix metalloproteinase inhibitors induce regression, and tenascin-C antisense prevents progression, of vascular disease. J Clin Invest. 2000;105:21-34.

Davidson JM, LuValle PA, Zoia O, Quaglino D, Jr., Giro M. Ascorbate differentially regulates elastin and collagen biosynthesis in vascular smooth muscle cells and skin fibroblasts by pretranslational mechanisms. J Biol Chem. 1997;272:345-52.

El-Ghannam A, Ducheyne P, Shapiro IM. Effect of serum proteins on osteoblast adhesion to surface-modified bioactive glass and hydroxyapatite. J Orthop Res. 1999;17:340-5.

Ferroni P, Basili S, Martini F, Cardarello CM, Ceci F, Di Franco M, Bertazzoni G, Gazzaniga PP, Alessandri C. Serum metalloproteinase 9 levels in patients with coronary artery disease: a novel marker of inflammation. J Investig Med. 2003;51:295-300.

Galis Z. Metalloproteases in remodeling of vascular extracellular matrix. Fibrinolysis & Proteolysis. 1999;13:54-63.

Galis ZS, Johnson C, Godin D, Magid R, Shipley JM, Senior RM, Ivan E. Targeted disruption of the matrix metalloproteinase-9 gene impairs smooth muscle cell migration and geometrical arterial remodeling. Circ Res. 2002;91:852-9.

Galis ZS, Khatri JJ. Matrix metalloproteinases in vascular remodeling and atherogenesis: the good, the bad, and the ugly. Circ Res. 2002;90:251-62.

Galis ZS, Muszynski M, Sukhova GK, Simon-Morrissey E, Unemori EN, Lark MW, Amento E, Libby P. Cytokine-stimulated human vascular smooth muscle cells synthesize a complement of enzymes required for extracellular matrix digestion. Circ Res. 1994;75:181-9.

Garcia AJ, Vega MD, Boettiger D. Modulation of cell proliferation and differentiation through substrate-dependent changes in fibronectin conformation. Mol Biol Cell. 1999;10:785-98.

Girton TS, Oegema TR, Grassl ED, Isenberg BC, Tranquillo RT. Mechanisms of stiffening and strengthening in media-equivalents fabricated using glycation. J Biomech Eng. 2000;122:216-23.

Giunchedi P, Conti B, Scalia S, Conte U. In vitro degradation study of polyester microspheres by a new HPLC method for monomer release determination. J Control Release. 1998;56:53-62.

Godin D, Ivan E, Johnson C, Magid R, Galis ZS. Remodeling of carotid artery is associated with increased expression of matrix metalloproteinases in mouse blood flow cessation model. Circulation. 2000;102:2861-6.

Gough JE, Christian P, Scotchford CA, Jones IA. Craniofacial osteoblast responses to polycaprolactone produced using a novel boron polymerisation technique and potassium fluoride post-treatment. Biomaterials. 2003;24:4905-12.

Grafe M, Auch-Schwelk W, Graf K, Terbeek D, Hertel H, Unkelbach M, Hildebrandt A, Fleck E. Isolation and characterization of macrovascular and microvascular endothelial cells from human hearts. Am J Physiol. 1994;267:H2138-48.

Griffith L. Polymeric biomaterials. Acta Mater. 2000;48:263-277.

Griffith LG. Emerging design principles in biomaterials and scaffolds for tissue engineering. Ann N Y Acad Sci. 2002;961:83-95.

Gugala Z, Gogolewski S. Protein adsorption, attachment, growth and activity of primary rat osteoblasts on polylactide membranes with defined surface characteristics. Biomaterials. 2004;25:2341-51.

Gurer G, Erdem S, Kocaefe C, Ozguc M, Tan E. Expression of matrix metalloproteinases in vasculitic neuropathy. Rheumatol Int. 2003.

Gurjar MV, Sharma RV, Bhalla RC. eNOS gene transfer inhibits smooth muscle cell migration and MMP-2 and MMP-9 activity. Arterioscler Thromb Vasc Biol. 1999;19:2871-7.

Hasirci V, Lewandrowski K, Gresser JD, Wise DL, Trantolo DJ. Versatility of biodegradable biopolymers: degradability and an in vivo application. J Biotechnol. 2001;86:135-50.

Haugland RPaIDJ. Intracellular Ion Indicator. Fluorescent and Luminescent Probes. 2nd ed: Academic press; 1999.

Heymans S, Luttun A, Nuyens D, Theilmeier G, Creemers E, Moons L, Dyspersin GD, Cleutjens JP, Shipley M, Angellilo A, Levi M, Nube O, Baker A, Keshet E, Lupu F, Herbert JM, Smits JF, Shapiro SD, Baes M, Borgers M, Collen D, Daemen MJ, Carmeliet P. Inhibition of plasminogen activators or matrix metalloproteinases prevents cardiac rupture but impairs therapeutic angiogenesis and causes cardiac failure. Nat Med. 1999;5:1135-42.

Huang S, Ingber DE. Shape-dependent control of cell growth, differentiation, and apoptosis: switching between attractors in cell regulatory networks. Exp Cell Res. 2000;261:91-103.

Ishii I, Tomizawa A, Kawachi H, Suzuki T, Kotani A, Koshushi I, Itoh H, Morisaki N, Bujo H, Saito Y, Ohmori S, Kitada M. Histological and functional analysis of vascular smooth muscle cells in a novel culture system with honeycomb-like structure. Atherosclerosis. 2001;158:377-84.

Itala A, Ylanen HO, Yrjans J, Heino T, Hentunen T, Hupa M, Aro HT. Characterization of microrough bioactive glass surface: surface reactions and osteoblast responses in vitro. J Biomed Mater Res. 2002;62:404-11.

Jackson CJ, Nguyen M. Human microvascular endothelial cells differ from macrovascular endothelial cells in their expression of matrix metalloproteinases. Int J Biochem Cell Biol. 1997;29:1167-77.

Jia MC, Schwartz MA, Sang QA. Suppression of human microvascular endothelial cell invasion and morphogenesis with synthetic matrixin inhibitors. Targeting angiogenesis with MMP inhibitors. Adv Exp Med Biol. 2000;476:181-94.

Johnson C, Galis ZS. Quantitative assessment of collagen assembly by live cells. J Biomed Mater Res. 2003;67A:775-84.

Johnson C, Galis ZS. Matrix metalloproteinase-2 and -9 differentially regulate smooth muscle cell migration and cell-mediated collagen organization. Arterioscler Thromb Vasc Biol. 2004;24:54-60.

Johnson C, Sung HJ, Lessner SM, Fini ME, Galis ZS. Matrix metalloproteinase-9 is required for adequate angiogenic revascularization of ischemic tissues: potential role in capillary branching. Circ Res. 2004;94:262-8.

Kanda S, Kuzuya M, Ramos MA, Koike T, Yoshino K, Ikeda S, Iguchi A. Matrix metalloproteinase and alphavbeta3 integrin-dependent vascular smooth muscle cell invasion through a type I collagen lattice. Arterioscler Thromb Vasc Biol. 2000;20:998-1005.

Kenney MC, Zorapapel N, Atilano S, Chwa M, Ljubimov A, Brown D. Insulin-like growth factor-I (IGF-I) and transforming growth factor-beta (TGF-beta) modulate tenascin-C and fibrillin-1 in bullous keratopathy stromal cells in vitro. Exp Eye Res. 2003;77:537-46.

Klee D, Ademovic Z, Bosserhoff A, Hoecker H, Maziolis G, Erli HJ. Surface modification of poly(vinylidenefluoride) to improve the osteoblast adhesion. Biomaterials. 2003;24:3663-70.

Kranzhofer A, Baker AH, George SJ, Newby AC. Expression of tissue inhibitor of metalloproteinase-1, -2, and -3 during neointima formation in organ cultures of human saphenous vein. Arterioscler Thromb Vasc Biol. 1999;19:255-65.

Kurata S, Hata R. Epidermal growth factor inhibits transcription of type I collagen genes and production of type I collagen in cultured human skin fibroblasts in the presence and absence of L-ascorbic acid 2-phosphate, a long-acting vitamin C derivative. J Biol Chem. 1991;266:9997-10003.

Kweon H, Yoo MK, Park IK, Kim TH, Lee HC, Lee HS, Oh JS, Akaike T, Cho CS. A novel degradable polycaprolactone networks for tissue engineering. Biomaterials. 2003;24:801-8.

Lantz GC, Badylak SF, Hiles MC, Coffey AC, Geddes LA, Kokini K, Sandusky GE, Morff RJ. Small intestinal submucosa as a vascular graft: a review. J Invest Surg. 1993;6:297-310.

Lee SH, Kim BS, Kim SH, Choi SW, Jeong SI, Kwon IK, Kang SW, Nikolovski J, Mooney DJ, Han YK, Kim YH. Elastic biodegradable poly(glycolide-co-caprolactone) scaffold for tissue engineering. J Biomed Mater Res. 2003;66A:29-37.

Lessner SM, Prado HL, Waller EK, Galis ZS. Atherosclerotic lesions grow through recruitment and proliferation of circulating monocytes in a murine model. Am J Pathol. 2002;160:2145-55.

Lewandrowski KU, Gresser JD, Wise DL, Trantolo DJ, Hasirci V. Tissue responses to molecularly reinforced polylactide-co-glycolide implants. J Biomater Sci Polym Ed. 2000;11:401-14.

L'Heureux N, Paquet S, Labbe R, Germain L, Auger FA. A completely biological tissue-engineered human blood vessel. Faseb J. 1998;12:47-56.

Li S, Garreau H, Vert M. Structure-Property relationships in the case of the degradation of massive poly (a-hydroxyl acid) in aqueous media, Part 3: Influence of the morphology of poly(L-lactic acid). J Mater Sci Mater Med. 1990;1:198-206.

Li S, Lao J, Chen BP, Li YS, Zhao Y, Chu J, Chen KD, Tsou TC, Peck K, Chien S. Genomic analysis of smooth muscle cells in 3-dimensional collagen matrix. Faseb J. 2003;17:97-9.

Lu L, Garcia CA, Mikos AG. In vitro degradation of thin poly(DL-lactic-co-glycolic acid) films. J Biomed Mater Res. 1999;46:236-44.

Lu L, Peter SJ, Lyman MD, Lai HL, Leite SM, Tamada JA, Uyama S, Vacanti JP, Langer R, Mikos AG. In vitro and in vivo degradation of porous poly(DL-lactic-co-glycolic acid) foams. Biomaterials. 2000;21:1837-45.

Mason DP, Kenagy RD, Hasenstab D, Bowen-Pope DF, Seifert RA, Coats S, Hawkins SM, Clowes AW. Matrix metalloproteinase-9 overexpression enhances vascular smooth muscle cell migration and alters remodeling in the injured rat carotid artery. Circ Res. 1999;85:1179-85.

Massia SP, Hubbell JA. Immobilized amines and basic amino acids as mimetic heparin-binding domains for cell surface proteoglycan-mediated adhesion. J Biol Chem. 1992;267:10133-41.

Matsuda T, Akutsu T, Kira K, Matsumoto H. Development of hybrid compliant graft: rapid preparative method for reconstruction of a vascular wall. ASAIO Trans. 1989;35:553-5.

Mavromatis K, Fukai T, Tate M, Chesler N, Ku DN, Galis ZS. Early effects of arterial hemodynamic conditions on human saphenous veins perfused ex vivo. Arterioscler Thromb Vasc Biol. 2000;20:1889-95.

Meredith J, Smith, AP, Karim, A, Amis, EJ. Combinatorial materials science: Thin-film dewetting. Macromolecules. 2000;33:9747-9756.

Meredith JA, EJ. LCST phase separation in biodegradable polymer blends: poly(D,L-lactide) and poly(-caprolactone). Macromol Chem Phys. 2000;200:733-739.

Meredith JC, Sormana JL, Keselowsky BG, Garcia AJ, Tona A, Karim A, Amis EJ. Combinatorial characterization of cell interactions with polymer surfaces. J Biomed Mater Res. 2003;66A:483-90.

Mikos AG, McIntire LV, Anderson JM, Babensee JE. Host response to tissue engineered devices. Adv Drug Deliv Rev. 1998;33:111-139.

Miller DC, Thapa A, Haberstroh KM, Webster TJ. Endothelial and vascular smooth muscle cell function on poly(lactic-co-glycolic acid) with nano-structured surface features. Biomaterials. 2004;25:53-61.

Miller RA, Brady JM, Cutright DE. Degradation rates of oral resorbable implants (polylactates and polyglycolates): rate modification with changes in PLA/PGA copolymer ratios. J Biomed Mater Res. 1977;11:711-9.

Mitchell IM, Essop AR, Scott PJ, Martin PG, Gupta NK, Saunders NR, Nair RU, Williams GJ. Bovine internal mammary artery as a conduit for coronary revascularization: long-term results. Ann Thorac Surg. 1993;55:120-2.

Nerem RM, Seliktar D. Vascular tissue engineering. Annu Rev Biomed Eng. 2001;3:225-43.

Niklason LE, Abbott W, Gao J, Klagges B, Hirschi KK, Ulubayram K, Conroy N, Jones R, Vasanawala A, Sanzgiri S, Langer R. Morphologic and mechanical characteristics of engineered bovine arteries. J Vasc Surg. 2001;33:628-38.

Niklason LE, Gao J, Abbott WM, Hirschi KK, Houser S, Marini R, Langer R. Functional arteries grown in vitro. Science. 1999;284:489-93.

Ochsner JL, Lawson JD, Eskind SJ, Mills NL, DeCamp PT. Homologous veins as an arterial substitute: long-term results. J Vasc Surg. 1984;1:306-13.

Ogle BM, Mooradian DL. The role of vascular smooth muscle cell integrins in the compaction and mechanical strengthening of a tissue-engineered blood vessel. Tissue Eng. 1999;5:387-402.

Park JC, Sung HJ, Lee DH, Park YH, Cho BK, Suh H. Specific determination of endothelial cell viability in the whole cell fraction from cryopreserved canine femoral veins using flow cytometry. Artif Organs. 2000;24:829-33.

Pauly RR, Passaniti A, Bilato C, Monticone R, Cheng L, Papadopoulos N, Gluzband YA, Smith L, Weinstein C, Lakatta EG, et al. Migration of cultured vascular smooth muscle cells through a basement membrane barrier requires type IV collagenase activity and is inhibited by cellular differentiation. Circ Res. 1994;75:41-54.

Perugini P, Genta I, Conti B, Modena T, Cocchi D, Zaffe D, Pavanetto F. PLGA microspheres for oral osteopenia treatment: preliminary "in vitro"/"in vivo" evaluation. Int J Pharm. 2003;256:153-60.

Prabhakar V, Grinstaff MW, Alarcon J, Knors C, Solan AK, Niklason LE. Engineering porcine arteries: effects of scaffold modification. J Biomed Mater Res. 2003;67A:303-11.

Pyne A, Chatterjee K, Suryanarayanan R. Solute crystallization in mannitol-glycine systems--implications on protein stabilization in freeze-dried formulations. J Pharm Sci. 2003;92:2272-83.

Pyo R, Lee JK, Shipley JM, Curci JA, Mao D, Ziporin SJ, Ennis TL, Shapiro SD, Senior RM, Thompson RW. Targeted gene disruption of matrix metalloproteinase-9 (gelatinase B) suppresses development of experimental abdominal aortic aneurysms. J Clin Invest. 2000;105:1641-9.

Rechinger KB, Siegumfeldt H, Svendsen I, Jakobsen M. "Early" protein synthesis of Lactobacillus delbrueckii ssp. bulgaricus in milk revealed by [35S] methionine labeling and two-dimensional gel electrophoresis. Electrophoresis. 2000;21:2660-9.

Rizzi SC, Heath DJ, Coombes AG, Bock N, Textor M, Downes S. Biodegradable polymer/hydroxyapatite composites: surface analysis and initial attachment of human osteoblasts. J Biomed Mater Res. 2001;55:475-86.

Ruef J, Rao GN, Li F, Bode C, Patterson C, Bhatnagar A, Runge MS. Induction of rat aortic smooth muscle cell growth by the lipid peroxidation product 4-hydroxy-2-nonenal. Circulation. 1998;97:1071-8.

Saltzman W. Growth-factor delivery in tissue engineering. MRS Bull. 1996;21:62-65.

Schliecker G, Schmidt C, Fuchs S, Wombacher R, Kissel T. Hydrolytic degradation of poly(lactide-co-glycolide) films: effect of oligomers on degradation rate and crystallinity. Int J Pharm. 2003;266:39-49.

Seliktar D, Black RA, Vito RP, Nerem RM. Dynamic mechanical conditioning of collagen-gel blood vessel constructs induces remodeling in vitro. Ann Biomed Eng. 2000;28:351-62.

Seliktar D, Nerem RM, Galis ZS. Mechanical strain-stimulated remodeling of tissue-engineered blood vessel constructs. Tissue Eng. 2003;9:657-66.

Shian SG, Kao YR, Wu FY, Wu CW. Inhibition of invasion and angiogenesis by zinc-chelating agent disulfiram. Mol Pharmacol. 2003;64:1076-84.

Shum-Tim D, Stock U, Hrkach J, Shinoka T, Lien J, Moses MA, Stamp A, Taylor G, Moran AM, Landis W, Langer R, Vacanti JP, Mayer JE, Jr. Tissue engineering of autologous aorta using a new biodegradable polymer. Ann Thorac Surg. 1999;68:2298-304; discussion 2305.

Silvestre JS, Mallat Z, Tamarat R, Duriez M, Tedgui A, Levy BI. Regulation of matrix metalloproteinase activity in ischemic tissue by interleukin-10: role in ischemia-induced angiogenesis. Circ Res. 2001;89:259-64.

Sleight P. Current options in the management of coronary artery disease. Am J Cardiol. 2003;92:4N-8N.

Suh H, Hwang YS, Lee JE, Han CD, Park JC. Behavior of osteoblasts on a type I atelocollagen grafted ozone oxidized poly L-lactic acid membrane. Biomaterials. 2001;22:219-30.

Sung H-J, C. Johnson, C and Galis, ZS. The effect of scaffold degradation rate on the three-dimensional cell growth and angiogenesis. Biomaterials. 2004;[Epub ahead of print].

Teebken OE, Bader A, Steinhoff G, Haverich A. Tissue engineering of vascular grafts: human cell seeding of decellularised porcine matrix. Eur J Vasc Endovasc Surg. 2000;19:381-6.

ter Brugge PJ, Wolke JG, Jansen JA. Effect of calcium phosphate coating composition and crystallinity on the response of osteogenic cells in vitro. Clin Oral Implants Res. 2003;14:472-80.

Thapa A, Webster TJ, Haberstroh KM. Polymers with nano-dimensional surface features enhance bladder smooth muscle cell adhesion. J Biomed Mater Res. 2003;67A:1374-83.

Therin M, Christel P, Li S, Garreau H, Vert M. In vivo degradation of massive poly(alpha-hydroxy acids): validation of in vitro findings. Biomaterials. 1992;13:594-600.

Thomson DA, CM. Athanasiou, KA. The effect of dynamic compressive loading on biodegradable implants of 50-50% polylactic acid-polyglycolic acid. Tissue Eng. 1996;2:61-74.

Tnasey W. Ultimate mammalian cell pulse-chase. Tansey lab protocol. 2002.

Tranquillo RT, Girton TS, Bromberek BA, Triebes TG, Mooradian DL. Magnetically orientated tissue-equivalent tubes: application to a circumferentially orientated media-equivalent. Biomaterials. 1996;17:349-57.

van Dijkhuizen-Radersma R, Roosma JR, Kaim P, Metairie S, Peters FL, de Wijn J, Zijlstra PG, de Groot K, Bezemer JM. Biodegradable poly(ether-ester) multiblock copolymers for controlled release applications. J Biomed Mater Res. 2003;67A:1294-304.

Washburn NR, Yamada KM, Simon CG, Jr., Kennedy SB, Amis EJ. High-throughput investigation of osteoblast response to polymer crystallinity: influence of nanometer-scale roughness on proliferation. Biomaterials. 2004;25:1215-24.

Weinberg CB, Bell E. A blood vessel model constructed from collagen and cultured vascular cells. Science. 1986;231(4736):397-400.

Wesley RB, 2nd, Meng X, Godin D, Galis ZS. Extracellular matrix modulates macrophage functions characteristic to atheroma: collagen type I enhances acquisition of resident macrophage traits by human peripheral blood monocytes in vitro. Arterioscler Thromb Vasc Biol. 1998;18:432-40.

Weyand M, Kerber S, Schmid C, Rolf N, Scheld HH. Coronary artery bypass grafting with an expanded polytetrafluoroethylene graft. Ann Thorac Surg. 1999;67:1240-4; discussion 1244-5.

Wieland M, Chehroudi B, Textor M, Brunette DM. Use of Ti-coated replicas to investigate the effects on fibroblast shape of surfaces with varying roughness and constant chemical composition. J Biomed Mater Res. 2002;60:434-44.

Xi XP, Graf K, Goetze S, Hsueh WA, Law RE. Inhibition of MAP kinase blocks insulin-mediated DNA synthesis and transcriptional activation of c-fos by Elk-1 in vascular smooth muscle cells. FEBS Lett. 1997;417:283-6.

Yang Y, Bumgardner JD, Cavin R, Carnes DL, Ong JL. Osteoblast precursor cell attachment on heat-treated calcium phosphate coatings. J Dent Res. 2003;82:449-53.

Zentner GM, Rathi R, Shih C, McRea JC, Seo MH, Oh H, Rhee BG, Mestecky J, Moldoveanu Z, Morgan M, Weitman S. Biodegradable block copolymers for delivery of proteins and water-insoluble drugs. J Control Release. 2001;72:203-15.

Zhang YH, Fang LH, Ku BS. Fangchinoline inhibits rat aortic vascular smooth muscle cell proliferation and cell cycle progression through inhibition of ERK1/2 activation and c-fos expression. Biochem Pharmacol. 2003;66:1853-60.

Zhang YM, Bataillon-Linez P, Huang P, Zhao YM, Han Y, Traisnel M, Xu KW, Hildebrand HF. Surface analyses of micro-arc oxidized and hydrothermally treated titanium and effect on osteoblast behavior. J Biomed Mater Res. 2004;68A:383-91.

VITA

Hak-Joon Sung studied in the Ph.D. program of Georgia Tech/Emory Biomedical Engineering beginning August 2001, under advisorship of Dr. Zorina S. Galis. He transferred to Dr. Larry V. McIntire's group in January 2004, as Dr. Galis was on a leave of absence.

Education and Experience

Yonsei University — Seoul, Korea

M.S. in Biomaterials of Tissue Engineering — Feb. 2001

B.A. in Biochemistry — Feb. 1999

Research and Teaching Assistant — 1999 ~ 2001

Department of Medical Engineering, College of Medicine, Yonsei University

Researcher — 1999 ~ 2001

Medical Technology and Quality Evaluation Center (MTEC) Yonsei Medical Research Center

Sergeant (Honorably discharged) — March 1995 ~ May 1997

Military Operations and Strategy Division in Artillery Battalion of the Korean Army

Publications

1. The effect of scaffold degradation rate on the three-dimensional cell growth and angiogenesis. Sung HJ, Meredith JC, Johnson C and Galis ZS.Biomaterials. 2004;[Epub ahead of print].

2. Matrix metalloproteinase-9 is required for adequate angiogenic revascularization of ischemic tissues: potential role in capillary branching. Johnson C, Sung HJ, Lessner SM, Fini ME, Galis ZS. Circ Res. 2004 Feb 6;94(2):262-8. Epub 2003 Dec 11.

3. Vascular oxidant stress enhances progression and angiogenesis of experimental atheroma. Khatri JJ, Johnson C, Magid R, Lessner SM, Laude KM, Dikalov SI, Harrison DG, Sung H-J, Rong Y, Galis ZS. Circulation. 2004 Feb 3;109(4):520-5. Epub 2004 Jan 26.

4. Liposomal entrapment of cefoxitin to improve cellular viability and function in human saphenous veins. Park JC, Suh H, Sung HJ, Han DW, Lee DH, Park BJ, Park YH, Cho BK. Artif Organs. 2003 Jul;27(7):623-30.

5. Antibacterial effect of antibiotic solution on cellular viability in canine veins. Park JC, Sung HJ, Lee DH, Park YH, Cho BK, Suh H. Artif Organs. 2001 Jun;25(6):490-4.

6. Specific determination of endothelial cell viability in the whole cell fraction from cryopreserved canine femoral veins using flow cytometry. Park JC, Sung HJ, Lee DH, Park YH, Cho BK, Suh H. Artif Organs. 2000 Oct;24(10):829-33.

7. Viability of cells in cryopreserved canine cardiovascular organs for transplantation. Park JC, Sung HJ, Lee DH, Park YH, Cho BK, Suh H. Yonsei Med J. 2000 Oct;41(5):556-62.

Publications in Process

1. Combinatorial screening of differential regulation of cell interactions on the surface of biodegradable polymer blends.[chapter 5]: Sung HJ, Su J, Berglund JD, Russ BV, Meredith JC and Galis ZS. Manuscript in preparation.

2. Matrix metalloproteinase (MMP)-9 facilitates cell-matrix interactions for function and survival of vascular constructs.[chapter 4]: Sung HJ, Johnson CE, Magid R, Lessner SM, Drury DN and Galis ZS. *Tissue Eng*; [in review].

3. Fluorescence microangiography : A method for quantitative functional and morphological characterization of native and angiogenic microvasculature. Johnson CE, Sung HJ, Lessner SM and Galis ZS. [Resubmission in preparation]